THERMAL MANAGEMENT OF HYBRID PHOTOVOLTAIC SYSTEMS

JONATHAN YONG KAI YEANG

**A project report submitted in partial fulfilment of the
requirements for the award of Bachelor of Engineering
(Honours) Mechanical Engineering**

**Lee Kong Chian Faculty of Engineering and Science
Universiti Tunku Abdul Rahman**

April 2021

DECLARATION

I hereby declare that this project report is based on my original work except for citations and quotations which have been duly acknowledged. I also declare that it has not been previously and concurrently submitted for any other degree or award at UTAR or other institutions.

Signature   :

Name   :   Jonathan Yong Kai Yeang

ID No.   :   1704613

Date   :   08/05/2021

APPROVAL FOR SUBMISSION

I certify that this project report entitled **"THERMAL MANAGEMENT OF HYBRID PHOTOVOLTAIC SYSTEMS"** was prepared by **JONATHAN YONG KAI YEANG** has met the required standard for submission in partial fulfilment of the requirements for the award of Bachelor of Engineering (Honours) Mechanical Engineering at Universiti Tunku Abdul Rahman.

Approved by,

Signature   :

Supervisor   :   Dr. Rubina Bahar

Date   :   08/05/2021

ACKNOWLEDGEMENTS

First and foremost, all praises to God for providing me with blessings and surrounds me with so many helpful and encouraging people throughout the whole development of this research.

I would like to thank everyone who had given me the support I need in completing this research project. All of your helps and contributions will always be remembered. I would also like to address my utmost gratitude to my research supervisor, Dr. Rubina Bahar for her guidance and enormous patience throughout the entirety of this research project. The way of how she communicates with me makes me feel comfortable without any feeling of being overwhelmed.

The completion of this research project would not be possible without the support of my lovely parents, who had always giving me encouragement whenever it was needed. I would also like to thank some of my close friends from church who are constantly caring for me despite everything that is going on with their life as well. Your words and supports are valuable to me, and I cannot express how much those words mean to me.

ABSTRACT

The photovoltaic cells are very sensitive to the temperature of their module. Any increase in temperature will largely affect the performance of the entire system. This is because heat can easily degrade any solar panel, causing it to produce lesser electricity when absorbing the same amount of solar radiation. This is why the studies of heat removal from its module are essential to optimize the performance of hybrid photovoltaic systems. Especially when Malaysia is at the equator with a hot-humid climate all year long. Although on certain occasions, the wind can provide additional cooling, it is still unreliable, to say the least, due to how unpredictable it comes. In this design, heat is transferred away from the collectors via water tubes, which lie underneath the glass panel. Two subsystems are joined to the collectors to utilize the heat generated. The primary subsystem is to heat a hot water storage tank, while the second subsystem is to provide space cooling into the interior household. At maximum solar irradiance, the temperature inside the water storage tank can rise to 43.8 °C, which requires further heating of 2.28 kWh to bring the temperature up to 50 °C. As for space cooling, the absorption refrigeration system can produce a maximum coefficient of performance at a value of 2.2. This subsystem will act as an additional application instead of replacing the air conditioner entirely due to how unreliable this system can be since the operating requirement is based on the availability of solar irradiance. With this hybrid photovoltaic system implemented, a breakeven point is calculated to be approximately one year. Although the hybrid photovoltaic system proposed has a high initial fixed cost, after a year, the cost of installing and operating installing the instant water heater and air conditioners will be more than the proposed system.

TABLE OF CONTENTS

LIST OF TABLES

LIST OF FIGURES

LIST OF SYMBOLS / ABBREVIATIONS

δ	Thickness, m
k	Thermal conductivity, W/m.K
L_1	Length of casing
L_2	Width of casing
L_3	Height of casing
V_{wind}	Wind velocity, m/s
α_a	Convective heat transfer coefficient, $W/m^2.K$
σ_{SB}	Stefan Boltzmann^' s constant, $W/m^2.K^4$
ε_g	Emissivity of the glass cover
ε_p	Emissivity of the absorber plate
β	Tilt angle of collector, °
N	Number of glass layer
T_m	Mean plate temperature of absorber, K
T_a	Ambient temperature, K
U	Overall heat transfer coefficient, $W/m^2.K$
A	Area of preheating heat exchanger, m^2
LMTD	Logarithmic mean temperature difference, K
S	Solar irradiance, W/m^2
F_R	Removal factor
U_L	Total loss coefficient, $W/m^2.K$
$\dot{Q}_L$	Total rate of heat loss by collector, W
$\dot{Q}_u$	Total rate of heat collected by collector, W
F_R	Removal factor
η	Collector efficiency
$\dot{m}$	Mass flow rate, kg/s
C_p	Specific heat capacity of water, kJ/kg.K
T_{out}	Temperature of outlet water, K
T_{in}	Temperature of inlet water, K
D_i	Inner diameter of tube, m
D_o	Outer diameter of tube, m
L	Length of tubes, m

N_p	Number of tube pass
N_t	Number of tubes
ρ	Density of tube fluid, kg/m^3
μ	Dynamic viscosity, Pa.s
ω_1	Inlet specific humidity, kg water/kg dry air
ω_2	Outlet specific humidity, kg water/kg dry air
$\dot{m}_a$	Mass flow rate of dry air, kg/s
$\dot{m}_w$	Mass flow rate of water vapour, kg/s
h_1	Inlet enthalpy of dry air, kJ/kg
h_2	Outlet enthalpy of dry air, kJ/kg K
h_w	Enthalpy of water vapour, kJ/kg
R	Gas constant of air, kJ/kg.K
T	Dry bulb temperature, K
P_a	Partial pressure of dry air, kPa
P_1	Atmospheric pressure, kPa
P_v	Partial pressure of water vapour, kPa
h_g	enthalpy of dry air, kJ/kg dry air
T_s	Temperature of heat source, K
T_l	Temperature of refrigerated space, K

LIST OF APPENDICES

CHAPTER 1

INTRODUCTION

1.1   General Introduction

With the rapid increase in energy usage during the past few decades, energy became one of the most important empowering sources that are essential for any further development of industries. Due to the high energy demand, any further increase in the usage of conventional energy, for example generating power using fossil fuels, will create a huge negative impact on the environment. Conventional energy is also finite, which raises concern with regards to its limitation source, leading to researchers needing to find an alternative.

Renewable energy is classified as the most sustainable energy that is able to meet the demand for energy without having any worries of a limited resource. Moreover, it is eco-friendly and is always available without any charges incurred. Nowadays, Malaysia is trying to attain sustainable energy development by promoting the usage of renewable energy at the highest level and giving supports to its investor. By comparing to other sustainable sources, solar power has the least concern regarding the installation location. This is because the size of solar photovoltaic panels is very small compared to hydroelectric dams or wind farms. Adding the fact that the panels are mostly installed on the roof, the solar panels will always absorb some solar radiation in the daytime even when part of the solar panels are blocked by other obstacles.

Malaysia is suitable for any development of solar industries. This is because it is located in the equatorial zone. On average, 4500 kWh/m2 of solar radiation were shone daily (P.D. Abd. Aziz et al., 2016). Despite having to meet this high demand for energy, Malaysia has the capability to generate even more than the current demand provided that every roof in Peninsula Malaysia has solar photovoltaic panels installed. Former minister Yeo Bee Yin, from the Ministry of Energy, Science and Technology in Malaysia, has mentioned that there are a total of 4.12 million buildings with a rooftop that can install solar panels, which could potentially generate up to 34194 MW of electricity (The ASEAN Post, 2019). With the advancement of technology, the cost of installing solar panels has been greatly reduced.

According to the research conducted by Ecavo (2021), by looking at the performance of regular solar panels, merely 14 % of energy is converted into electricity on residential buildings. Even for panels that are following the movement of the sun, the efficiency will never reach 100 %, the most it can achieve is only 85 %. For a non-trackable sunlight system, the maximum achievable efficiency is even lower, only 55 % will be converted into electricity. The reason behind the low efficiency is due to the degradation in cells caused by heat being generated in the solar panels after long exposure to solar radiation. The higher temperature in cells caused the dropped in voltage, where it results in the dropped in overall power.

1.2   Importance of the Study

With the superb rise in the usage of photovoltaic cells in Malaysia, the performance of these photovoltaic cells has been the main focus. Studies have stated that the amount of solar radiation that has been utilized directly that converts to electricity are only ranging from 10 % to 20 % (Tao Ma et al., 2019). Most of the remaining energy is diffused as heat, thus increasing the temperature of the photovoltaic cells which leads to a problem like reduction in power and degradation of photovoltaic cells (Tao Ma et al., 2019). Electrical efficiency has a negative correlation with the temperature of photovoltaic cells.

Most of this research project will be focusing on the improvement of thermal management on the new hybrid photovoltaic system. Moreover, the cooling processes and the extraction of the heat generated then reusing this heat on other applications will be further explored. This will ultimately improve the electrical performance of the photovoltaic system and has a significant impact on the conservation of energy sources.

1.3   Problem Statement

The photovoltaic cells are very sensitive to the temperature of their module. Any increase in temperature will largely affect the performance of the entire system. This is because heat can easily degrade any solar panel, causing it to produce lesser electricity when absorbing the same amount of solar radiation. This is why the studies of heat removal from its module are essential in order to optimize the performance of hybrid photovoltaic systems. Although on certain occasions, the wind is able to provide additional cooling, it is still unreliable, to say the least, due to how

unpredictable it comes. Not to mention, any hot-humid weather is able to degrade the solar panels over their lifetime (Solar, 2019). Therefore, it is important to look at the climate from different regions and came up with designs that are beneficial even in the worst possible area.

Malaysia is a great example to start with since it has hot-humid weather all year long. The temperature is averaging in the range of 20 °C to 30 °C, with a higher average temperature between the month of April to August, which reaches up to 31.3 °C (Travelonline, 2020). Depending on the region, some regions experienced monsoon season sooner. Based on the data provided by Travelonline, the highest rainfall experienced is in November. Peninsular Malaysia have an average rainfall of 2500 mm annually, while East Malaysia has experienced higher average rainfall, up to 5080 mm annually. Once again, referring to the same statistic, between April and October, the hot-humid weather will occur more frequently due to its high temperature and rainfall between these months. During these months, the degradation caused by the heat and the humidity is far more severe as compared to other months, which is why it is important to manage the temperature of its module wisely. This, however, had given Malaysia a great opportunity to explore designs that are involving heat extractions since it has suitable locations for the development of solar industries.

From these problems, the design of photovoltaic systems had shown its limitation and have proven that it can be further improved in order to maximize its performance. The hybrid photovoltaic systems are then implemented to increase the efficiency and reliability of what a regular solar photovoltaic system failed to achieve. Hybrid referred to the combination of solar power with any other power generating energy source. There are many types of hybrid photovoltaic systems, but since the temperature of photovoltaic cells plays a major role in performance, one hybrid system that solved the thermal issue is known as a hybrid solar photovoltaic thermal system. The addition of a solar thermal collector will help with transferring any waste heat generated from the photovoltaic cells to a heat transfer fluid. This will ultimately lower the temperature of the entire photovoltaic modules, thus improving the performance.

1.4   Aim and Objectives

The aim of this study is to improve the thermal cooling of the hybrid photovoltaic system. This can be achieved by following several objectives, which is shown below:

1. To evaluate the heat transfer from the hybrid photovoltaic cooling system.
2. To design a combined heating and cooling system for utilizing the generated waste heat.
3. To analyse the performance of the combined setup in terms of cost and energy savings.

1.5   Scope and Limitation of the Study

The main scope of the study is to extract any heat generated from the photovoltaic cells, which will eventually decrease the electrical efficiency. However, there are several limitations in this study that could potentially decrease the accuracy of any results obtained. Such limitations are stated below:

- The location of the photovoltaic cells installed will result in different amounts of solar radiation absorbed by the cells. This includes altitude which will lead to obtaining varying results for heat generation.
- Wind velocity plays a major role in terms of cooling the photovoltaic cells. The seasonal changes will have a huge variation in climate throughout the year, which will generate different result corresponding to the season.

1.6   Contribution of the Study

This hybrid photovoltaic system may help in cooling the photovoltaic collector while utilizing any excessive heat generated for different types of applications. Having a lower temperature of photovoltaic thermal collector will result in higher efficiency on the amount of electricity produced. Not to mention, the hybrid photovoltaic systems can also save up some of the electricity consumption for the applications.

1.7   Outline of the Report

Literature review is analysed and discussed in Chapter 2 before selecting the proposed design for each system which will be discussed in Chapter 3. The results obtained from the proposed design are recorded and discussed in Chapter 4. The conclusions and recommendations of the overall findings will be discussed in Chapter 5.

CHAPTER 2

LITERATURE REVIEW

2.1   Introduction

The current study is mainly focusing on the temperature of the photovoltaic collector. Therefore, different types of cooling process are observed and reviewed to ensure that heat does not return to the collector.

2.2   Literature Review

Articles were chosen to be reviewed based on the potential effect it will bring toward the current study. Starting from observing the overall hybrid photovoltaic system, to each component such as the photovoltaic module and solar collector, before reviewing each subsystem that may have caused the change in temperature of the photovoltaic module. Three heat transfer process is also reviewed in order to observe the temperature of each section in the overall system. The application of the heat generated from the collector will be looked into detail to verify that heat will not return back to the system. The last section reviewed shows minor importance to current study, as it is mainly on the improvements on the design created by previous literatures.

2.3   Low-Grade Trigeneration System

The low-grade trigeneration system involves the process of cooling, heating and power the low-grade heat, which is for heat that has a temperature lower than 200 °C. Li, et al. (2020) has proposed a design that combines the solar absorption-subcooled compression hybrid system that is able to utilize heat at 60 °C, together with photovoltaic collectors which make the entire system having a trigeneration process. In this design, both the electricity and heat are produced at the same time by the photovoltaic collector whenever they are exposed to solar irradiation. The heat generated will drive the absorption subsystem and produced an output that serves as a subcooling power which will be used in the compression subsystem, thus reducing the compressor work. As for the heating process, the main usage is for preheating the water stored in the domestic hot water tank so that it can lower the electricity consumption of operating the heat pump. When the water temperature inside the storage tank is not

sufficient to drive the absorption subsystem, this heat generated from the photovoltaic collector is used to preheat the domestic hot water stored. According to the result obtained, the specific annual primary energy saving for this design is calculated to be 448.9 kWh/m^2. Li, et al. (2020) has also mentioned that the limiting factor for their design is the availability of roof-space, since the optimum system design can reach up to an area of 600 m^2. Therefore, in order to reduce the payback period, the authors have recommended to install as many photovoltaic thermal collectors as possible. By taking Zhuhai, a city in China with a solar irradiation of 1400 kWh/m^2 as the location to predict the minimum payback period, it will take 11.8 years to reach the break-even point.

Raja and Huang (2020) mentioned that when heating and cooling is involves in the generation of electric power process, it is then considered to be a trigeneration system. Their design is intended for multigeneration system, however by looking solely on the trigeneration system alone, it consists of essential subsystems such as the solar photovoltaic thermal collector, parabolic trough solar collector, thermal energy storage, single effect absorption cooling system and also a heat pump cycle. The authors also stated that some of the heat generated from the parabolic trough solar collector will be utilized in the absorption cycle for cooling. As for the heating process, the heat generated from the collector is stored in the thermal energy storage and will be used for space heating. The result obtained by the authors will not be further analysed as it is for multigeneration system instead of a trigeneration system.

Chen, et al. (2019) proposed another design for trigeneration system. In his design, internal combustion engine is added to the subsystem, main usage is for generating electricity by combusting the natural gas together with air. Another difference in design is the photovoltaic thermal collector used. Chen, et al. (2019) are using a compound parabolic concentrated-photovoltaic thermal solar collector, CPC-PVT instead of a regular photovoltaic collector. This is because CPC-PVT occupies lesser space and requires lower investment cost since it is able to adopts the low-concentration-ratio reflectors. The remaining subsystem is actually similar to the design proposed by Raja and Huang (2020), which consist of an absorption heat exchanger coupled with a thermal energy storage. The working condition for cooling process in this trigeneration system has many involvements of valves used. The absorption heat exchanger is able to produce chilled water for the purpose of space

cooling as well as for the generation of domestic hot water. As mentioned previously on including many valves in the design, there are valves that can control the flow of fluid so that the heat transfer is able to take place in order to generate the refrigerant water which flow to the low-pressure generator to has its heat removed. The remaining valves are used for controlling the path of the flow of refrigerant, which is varying depending on different conditions. For example, in a case where there is an excess amount of waste heat in the system, in order to transfer the excessive waste heat to the thermal energy storage, corresponding valves that are affecting the path of flow into the storage tank must be open. On the contrary, for the condition of having no excess waste heat, valves controlling the path of driving both the exhaust gas and mixed hot water to the absorption heat exchanger are opened. This also explains that there are several paths where the heat is able to be transferred in the system. As for the heating condition, the operations states are actually similar to the cooling working condition. The only difference involve is the path of fluid flow, which is to the high-pressure generator with another heat exchanger.

2.4   Photovoltaic Thermal Solar Collector

In the trigeneration system proposed by Li, et al. (2020), the photovoltaic thermal collector is glazed and laminated with ethylene-vinyl-acetate layers. The photovoltaic cells and absorber sheets are also coated with low-emissivity materials so that the thermal efficiency will be enhanced. Despite the fact that the installation of glass cover will reduce the electrical efficiency, it is able to reduce the heat loss. Based on the findings from Li, et al. (2020), the annual electrical efficiency of the photovoltaic thermal collector is 21 % lower than the photovoltaic module. This is mainly due to the installation of the additional glass cover that has a low-emissivity coating, which result in optical losses. On the same findings, Li, et al. (2020) mentioned that the total efficiency of photovoltaic thermal collector is 3.4 times more than the photovoltaic modules, which is due to the great energy utilization by transferring the heat away from the collector. The specific annual electricity saving of the design proposed is higher than the photovoltaic modules by 17.3 %.

Li, et al. (2020) proposed a design that places the photovoltaic thermal module next to the solar thermal collector in series which improves the electrical efficiency. Both of these components are mentioned to have an area of 1.645 m^2. The photovoltaic

thermal module consists of a glass cover, the absorber layer, a photovoltaic module, tubes and insulation. The solar thermal collector consists of the same layers, only with the exception of photovoltaic module. This photovoltaic module used has a model name that is labeled as JKM285PP-60-DV, which is manufactured by Jinko Solar. This module contains 60 polysilicon solar cells that has a maximum power output at 285 Wp and with a nominal efficiency of 17.8 %. A thickness of 0.025 m is reserved for the placement of air duct in between the glass cover and the photovoltaic module. Similar thickness of air duct is placed in solar collector. A total of ten identical tubes with a diameter of 0.01 m are placed parallel to each other with an offset of 0.1 m under the absorber layer. These tubes are also surrounded by the insulation layer, which is to prevent any heat from spreading into the ambient. For the remaining findings from the authors, it is mainly focusing on comparing the performance on different types of photovoltaic thermal solar collector. Four different combinations were stated by Li, et al. (2020), which are glazed PVT collector with a glazed ST collector, unglazed PVT collector with a glazed ST collector, glazed PVT with unglazed ST collector and lastly between both unglazed components. The authors then used these conditions to generate the thermal resistance network diagram for all cases and also a 2D transient mathematical model corresponding to each condition. Based on the findings, the authors concluded that the conditions where both of the components are unglazed will have a higher electrical efficiency. However, looking at a whole, the glazed PVT with a glazed ST collector has the best performance in terms of the overall energy efficiency and exergy efficiency.

Based on the design proposed by Ramdani and Ould-Lahoucine (2020), the photovoltaic thermal collector has a water-based design that is installed at the bottom of the direct absorption solar collector. As for the hybrid photovoltaic module, it contains a rectangular channel that is subjected to the flow of water. The top wall of this channel is covered with a glass that has a transmissivity of 90 %, as for the bottom wall, an insulated photovoltaic module is inserted. The working principle of the photovoltaic collector is as followed, started with the solar irradiation reaching the upper surface of glass plate and penetrates through the glass and reach the cooling water region. Water inside this region is fully developed and able to absorbed the infrared radiation.

Hottel and Woertz (1942), have generated equations that are used for calculating the convective and radiation loss result from the surface to the ambient and also the reflected solar radiation which caused by the transmissivity through glass surface. The heat loss can also be separated into three different sections, which are the heat loss from bottom, heat loss from side and heat loss from top of the solar collector.

As for the heat transfer occurring at the interfaces of water on both sides of the glass-plate, Ramdani and Ould-Lahoucine (2020) have identified that the convection occurred has a forced-convection nature, in which the Nusselt numbers can be calculated with the consideration of a fully developed laminar flow in between two parallel plates. The bottom section of the photovoltaic panel is assumed to be adiabatic. The authors have found out that the cooling channel height in the photovoltaic module will affect the overall efficiency. With the same water inlet velocity throughout the simulation, subjected to a solar irradiation of 1000 W/m^2 with the ambient temperature maintaining at 34 °C, it is observed that with any increase in channel height, the overall energy is shown to be higher. However, the exergy efficiency will decrease with the height of channel which produced a counter effect from the objective. Therefore, Ramdani and Ould-Lahoucine (2020) have identified that the optimum cooling channel height is 3.61 cm. This is obtained by finding the inflection point from new function the represents the difference between overall energy efficiency and the overall exergy efficiency. The authors then claimed that the optimum channel height calculated is accurate since it lies between the range of 3 cm to 4 cm, which is mentioned by Al-Shohani, et al. (2016) in a similar proposed design. Ramdani and Ould-Lahoucine (2020) further claimed that with the consideration of light weight, high infrared absorption and ease of flow circulation on extracting the produced heat, a height of 3.6 cm for the cooling channel has seems to be a good compromise.

Zarei, et al. (2020) has proposed a similar design on the photovoltaic modules. A monocrystalline panel is used on the solar electrical cooling since it performs better comparing with other systems. In their studies, the design of their photovoltaic thermal module is only focusing on the cooling processes, since the heating criteria will lower the electrical efficiency considerably. Due to the removal of heat pump or any relevant components for heating, the photovoltaic module will have its cooling channel connecting to two other heat exchangers. By looking solely on the design of the photovoltaic module, the placement of the cooling channel is different from the design

proposed by Ramdani and Ould-Lahoucine (2020). The glass panel is installed directly above the photovoltaic module, and the cooling channel is underneath this photovoltaic module. Zarei, et al. (2020) also concluded that the cooling process implemented on the photovoltaic panel will enhance the coefficient of performance up to 5.25 %.

A finding on improving the electrical performance by Pang, et al. (2020) described their design to be a crystalline silicon heterojunction with an intrinsic thin-layer photovoltaic module, which is also known as HIT-PV. The crystalline silicon HIT-PV were proposed due to the fact that it is cheap yet able to achieve a high efficiency. This brand new photovoltaic thermal system consists of a cooling plate that contains straight channels as well as helical channels. The entire cooling plate is made of aluminum and will result in achieving better electrical performance. As for the design proposed, the authors have decided to replace the polyethylene terephthalate with the aluminum collector which is confined in the vacuum lamination that has a dimension of 1645 mm × 985 mm. In both the HIT-PVT and HIT-PV module, there is a total of 60 pieces of HIT solar cells used. The HIT-PVT module is placed on top of the aluminum collector and is glued together with an adhesive called ethylene-vinyl-acetate. A dense oxide layer is formed on the top surface of the aluminum collector by anodic oxidation in order to achieve the electric insulated state. Pang, et al. (2020) has concluded that their results obtained on the measured output power as well as the electrical performance caused by the HIT-PVT module has a small increase of more than 5 % and 9 % respectively. The thermal efficiency achieved is around 34 % and it is calculated to have a primary energy saving as much as 79 %.

Su, et al. (2016) have recommended the usage of phase change material in replacing the cooling fluid. However, Abdelrazik, et al. (2019) have mentioned that the thermal conductivity for a phase change material is quite low, which may result in resistance during heat transfer. The authors further implied that the problem stated can be resolved by simply adding nanoparticles that have good thermal properties into the phase change material. In the design proposed by Liu, et al. (2017), the authors have decided to use microencapsulated phase change slurry as the cooling fluid, also known as MPCS which is mentioned to have a good thermal conductivity. Su, et al. (2016) have also mentioned that the PV/T system with MPCS has better performance when compared to any water-based PV/T and also air-based PV/T systems. However, there are limitations on the working condition of MPCS, as different climate temperature

may have prevented the slurry from melting. The authors suggested that changing the MPCS by considering the melting point based on different season is able to solve such issue. Figure 2.1 shows the PV temperature comparing two different coolants flowing along the PV module, which are the MPCS and water.
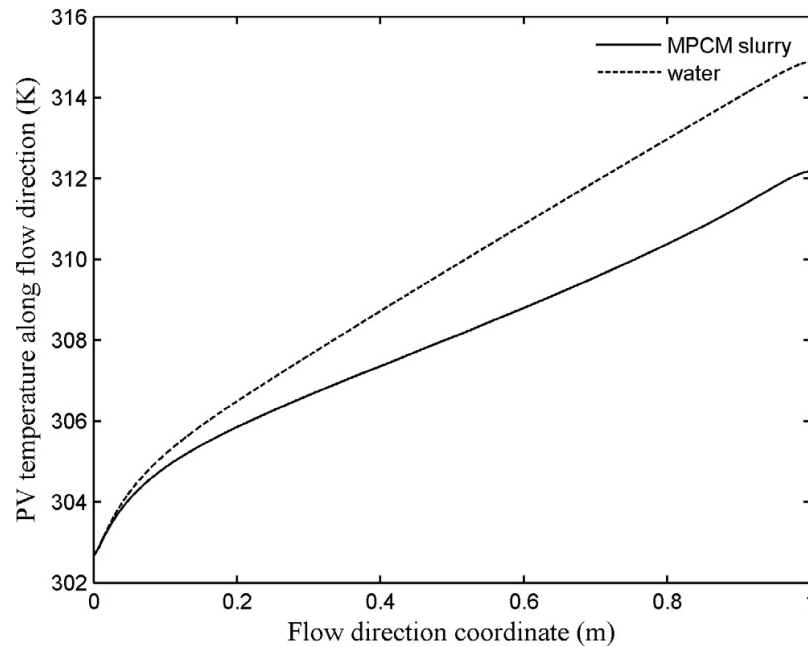
Figure 2.1: Temperature of PV with different coolants. (Liu, et al. 2017)

From Figure 2.1, it is obviously shown that the usage of MPCS will always result in lower PV temperature when compare to water. This is because MPCS have larger latent heat than water, which result in slow temperautre increment. Due to this, using MPCS has more benefits in terms of cooling since the temperature rose slower which caused the entire temperature of PV panel to fall as well, thus increasing the electrical efficiency. Liu, et al. (2017) have also mentioned that the outlet temperature of the slurry is lower than water, due to the high capacity of heat storage in MPCS, thus resulting in higher thermal efficiency. With these results obtained, the authors claimed that MPCS does indeed, have better heat removing capability comparing with water and air.

2.5   Hot Water Storage Tank

Hot water storage tank is required in a hybrid photovoltaic system in order to transfer the heat generated on the solar collector through a water channel that is connected to this tank, where the hot water is stored before processing for domestic uses. Abdullah, et al. (2020) stated that the hot water storage tank is often placed at ground level for a water-based photovoltaic thermal system. This tank is connected to two tubes, an inlet tube and an outlet tube which forms a closed loop system. The hot water storage tank requires higher temperature of water supplied into the tank through the inlet tube in order to undergo heat transfer. Thinsurat, et al. (2020) have mentioned that any increase in inlet temperature will result in a decrease in electrical performance of a photovoltaic module due to higher collector temperature. On a positive side, there is little to no energy storage loss since the tank contains good insulation. The trigeneration cycle proposed by Li, et al. (2020) contains a cylindrical vessel that act as a hot water storage tank. The authors are also able to generate a mathematical equation for calculating the energy balance by dividing the hot water storage tank into three equal volume sections.

The series configuration of connecting photovoltaic thermal collector with solar thermal collector designed by Ma, Li and Kazemian (2019) consist of a heat exchanger inside that hot water storage tank that is able to cool down the high temperature of water exiting the solar collector. As a result, the water flowing back into the photovoltaic thermal collector has a lower temperature to be reused again for the same purpose while having a hot water transferred out of the system for domestic usage. In the multi-generational system proposed by Raja and Huang (2020), heat exchanger was also used in organic Rankine cycle for the same purpose stated by Ma, Li and Kazemian (2019).

Li, et al. (2020) have involve the installation of heat exchanger in the trigeneration system. It is placed below the domestic hot water tank with the main purpose for exchanging heat with the water before it enters the storage tank. A preheating process is made possible by using the heat generated from the solar radiation on the photovoltaic thermal collector, which will ultimately reduce the electrical consumption on compression chiller and heat pump. Applying the concept of heat exchanger, the area of heat transfer can be calculated for a system with known temperatures and rate of heat transfer.

2.6   Absorption-Compression Subsystem

2.6.1   Solar Absorption-Subcooled Compression with Hybrid Cooling System

A different absorption-compression subsystem is proposed by Li, et al. (2020) which involves in a hybrid cooling system that can use the low-grade heat produced at around 60 °C efficiently. This subsystem is called SASCHCS that represents the solar absorption-subcooled compression with hybrid cooling system. The main reason that the authors decided to use SASCHCS as their subsystem is because of the elevated evaporation temperature, which often stays at 20 °C, will result in obtaining higher temperature for chilled water in the absorption subcycle. Furthermore, Li, et al. (2020) have also stated that the increased in evaporator temperature will result in the decreased in required temperature of any generator, from 75 °C to 55 °C which is as much as 20 °C. This will ultimately reduce the operating temperature of a photovoltaic thermal collector as the temperature of the input heat has been lowered by 20 °C, similar to the reduction in the required generator temperature. Based on the results obtained by Li, et al. (2020), the compressor work has reduced by 22.2 % on a sunny day with the implementation of SASCHCS. As mentioned previously on the great utilization of low-grade heat, the authors verified this statement by combining the photovoltaic thermal collector with SASCHCS in a trigeneration system. From their findings, SASCHCS will result in lower electrical efficiency since the implementation of this subsystem will also increase the operating temperature of the whole photovoltaic module. Not only that, photovoltaic thermal collector must have more layers of glass cover, which will result in optical loss thus affecting the electrical performance. Li, et al. (2020) have also mentioned the specifications of their absorption-compression subsystem. The absorption subsystem contains single-effect lithium bromide/water or ammonia/water inside the absorption chiller while the compression chiller contains R410a refrigerant. As for the compression chiller, it is directly connected to the electric grid so that the electricity generated from the photovoltaic thermal collector will be consumed. The authors then validate their simulation models proposed by comparing the results obtained from both the theoretical and experiment result before comparing them to find the differences. The results obtained for the coefficient of performance in the absorption subsystem, has an experimental and theoretical result of 0.567 and 0.594 respectively, with a difference of only 4.8 %. Similarly, the coefficient of performance of the compression subsystem

obtained are 6.41 and 6.59 for experimental and theoretical result respectively, with a slight deviation of 2.8 %. After verifying the simulation models used, the authors then carried a test by adding the absorber-compression subsystem into the trigeneration cycle. Having a result that is near to the measured data, the authors then implied that the SASCHCS can be well driven by low-grade solar heat generated from the photovoltaic thermal collector, thus resulting in high efficiency.

2.6.2 Heat Pump Design

The heating cycle can also be known as heat pump. Emmi, et al. (2020) revealed that heat pump is used to help in the production of domestic hot water before it is stored in the hot water storage tank. Apart from this usage, the authors also mentioned that heat pump can provide space cooling and also any space heating to residential building. Since heat pump is able to raise any temperature of water transferred from solar thermal collector before entering the domestic hot water tank, the temperature of solar thermal collector will be lower and so does the required operating temperature of photovoltaic module. This will result in better electrical performance. However, one drawback is that in order to power up the heat pump, it requires electrical demand obtained from the electrical energy generated by the photovoltaic module.

Dannemand, et al. (2020) have mentioned that the heat pump used in their design has a model name of NIBE F1155-6 which have a thermal output of 0 °C from the inlet and 35 °C at the outlet. This heat pump will require an electrical power consumption of 0.67 kW at 50 Hz frequency, and can power a thermal output as high as 3.15 kW. There is also a low standby electrical consumption of 19 W even when the heat pump is not in operation.

2.7 Heat Transfer

Su, et al. (2016) mentioned that any heat absorbed in the glass cover will be dissipated by conduction. Heat will be transferred from the glass cover to the surface of the photovoltaic cell through conduction. Looking at the design they proposed, the phase change material layer is placed underneath the backplane, which also lies below the photovoltaic module. The authors stated that the heat exchange in the PCM layer is mainly due to conduction. Su, et al. (2016) even added that the heat transfer through

convection between the PCM layer and the liquid channel is too insignificant when compared to the heat transfer through conduction.

The hybrid solar photovoltaic thermal system integrated with thermochemical sorption storage system which is designed by Thinsurat, et al. (2020) consist of an air gap mainly for the purpose of insulation. This will prevent any heat transfer from the glass cover to the photovoltaic cell through conduction, as the air gap is placed in between these two layers. As a result, the heat loss is minimized and produced a higher output temperature which improves the thermal performance. Similar to what Su, et al. (2016) mentioned, Thinsurat, et al. (2020) stated that the heat transfer is dominated by conduction for every solid element such as glass cover, absorber and photovoltaic cells.

For the design by Ma, Li and Kazemian (2019), there is also a layer of air duct right underneath the glass cover, similar to the design by Thinsurat, et al. (2020). The heat transfer via convection is only occurring inside the air duct of a solar collector, which is placed in between the glass cover and the photovoltaic module inside the photovoltaic thermal collector, and also in between the glass cover and absorber inside the solar thermal collector. They have also separated the calculation for radiative heat transfer coefficient into two sections. These are for radiative coefficient between the sky and glass cover and also between the glass cover and the corresponding components that lies underneath the glass cover of a collector. This means that for photovoltaic thermal collector, it is between the glass cover and a photovoltaic module whereas for solar thermal collector, it is between the glass cover and absorber.

2.8   Effects on Electrical and Thermal Performance

Zaite, et al. (2020) investigated the effect of night radiative cooling in a solar hybrid photovoltaic system have also noted down that the electrical performance of photovoltaic module increases gradually when the mass flow rate is increased. This is because the increased in mass flow rate is able to cool down the collector temperature, thus producing a higher electrical efficiency. Based on the results obtained by Abdullah, et al. (2020), increasing the mass flow rate from 2 LPM to 6 LPM will have an increased of electrical efficiency at a solar irradiance of 1000 W/m^2, from 6.69 % to 8.78 % for their proposed design, which is a water-based hybrid photovoltaic system.

For a water-based hybrid photovoltaic system, Ramdani and Ould-Lahoucine (2020) revealed that the inlet velocity has a positive impact on overall energy

efficiency but will result in lower exergy efficiency. The authors have further investigated on the velocity caused by wind, which stated higher wind velocity will lower the energy efficiency of the photovoltaic thermal collector. However, it is mentioned that the decrease in efficiency is too small to be considered significant.

Abdullah, et al. (2020) and Ramdani and Ould-Lahoucine (2020) have both concluded that increasing solar irradiation will have a favourable effect on thermal efficiency. This effect however, will reduced the electrical efficiency of the photovoltaic module as the increased in solar radiation will result in a temperature increase in photovoltaic unit (Abdullah, et al., 2020).

2.9 Summary

Since the main objective for this research is to analyse the thermal management of the hybrid photovoltaic system, any design that result in gaining the temperature of photovoltaic module is ignored. Although MPCS has a better heat response compared to water, water will be the selected heat carrier as it provides more application to be used further on. Adding the fact that MPCS has higher density than water, the whole content will be heavier with the same volume. Subsystem that used the electrical power generated by the photovoltaic module is not neglected in the current study unless it raises the temperature of the photovoltaic module. For an absorption subsystem, since generator requires high temperature of water input from the solar collector, the only downside is on the effectiveness of cooling for the PVT collector as the return temperature can be quite high. However, it does not increase the temperature of a PVT collector. Also, due to the vast range of applications provided from the trigeneration system, it is too important to neglect. Therefore, any design that involves in trigeneration cycle will be considered. As for the compression subsystem, it is ignored in the final design. This is because compressor requires an additional electricity power to run which is shown to be less efficient. Heat transfer process is one major focus in calculating the heat generated in each section inside the system. The remaining subsections are also important since each of the subsystems stated have involves heat transfer, which have to be carefully studied in order to determine the temperature of the photovoltaic module. The only exception is the organic Rankine cycle proposed by Raja and Huang (2020), which is a multigenerational cycle. Since this is already beyond the current objective, this cycle is ignored.

CHAPTER 3

METHODOLOGY AND WORK PLAN

3.1   Introduction

This chapter will be focusing on the methodology and also the work plan for the current research. The information used in reviewing literatures from previous section was used in generating the methodology for the current research.

Most of the workload for the first part of the research involves in designing the suitable hybrid photovoltaic system. After reviewing each literature and learning the concepts and working principle of every cycle of subsystems involved, the overall system can then be defined. With a whole system present, the material used by each component can be selected to fit the current design.

The second part of the research will be carried on much later, which will mostly be focusing on the results obtained from calculation. By using the equations that will be stated later on this chapter, rate of heat transfer for each component will be calculated in order to obtain the dimensions required for the heat exchanger. The heat loss from the solar collector which is dependant on the solar irradiance can also be calculated in order to find the output temperature of the water passing through the channel inside the collector. At the same time, the collector efficiency and collector removal factor are calculated to evaluate the performance on both the photovoltaic thermal collector and the solar thermal collector. For every applications implemented in the system, the output is calculated to ensure that all applications are feasible. Once the results obtained are verified to be accurate and acceptable, discussion is then able to make on every obtainable results, concluding the project by mentioning the effects while suggesting any recommendations on the findings. An illustration of the work plan is shown in the form of flow chart labelled as Figure 3.1.
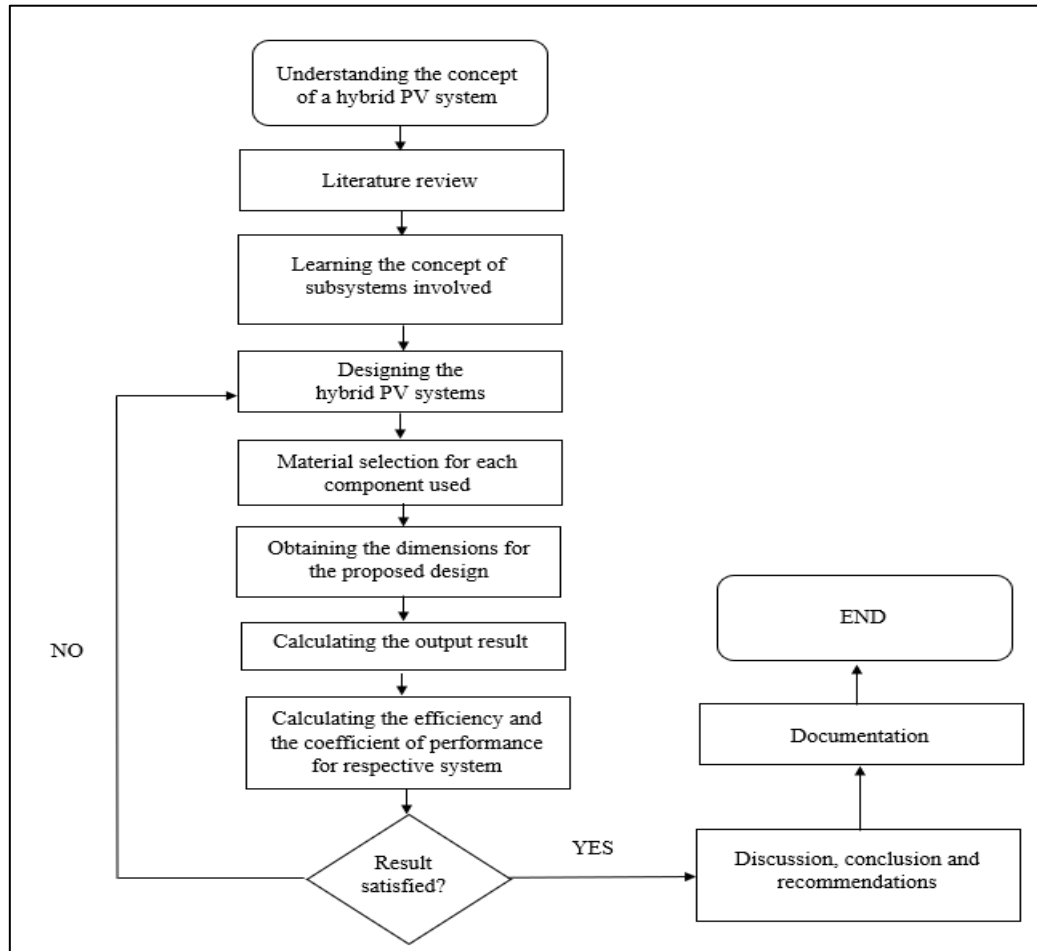
Figure 3.1: Process flow chart.

3.2 Methodology

All the components used in the system chosen will be examined in terms of their working principle, material used and also regions with heat loss.

3.2.1 Working principle of the hybrid Photovoltaic system

From the summary section on the previous chapter, it is mentioned that any trigeneration cycle design is considered despite the needs of higher operating temperature from the collector. This is because space cooling and preheating water storage tank act as an additional uses for reusing the extracted heat generated inside the solar collector. With this implication, only the compression subsystem is ignored as the vapour compression refrigeration cycle requires an additional electric power on the compressor. This means that any design with heat pump will still be ignored as well. The overall system is shown in Figure 3.2.

Figure 3.2: Schematic diagram for the main system.

Figure 3.2 shows the schematic diagram for a hybrid photovoltaic system with the photovoltaic thermal module coupled directly together with the solar thermal collector. The outlet tube is then connected to a storage tank that act as a heat exchanger. The working principle is listed as follow. Both the PVT collector and ST collector are exposed to sunlight and absorbed the solar radiation. For the PVT collector, despite the fact that most solar radiation is converted to electricity, low-grade heat is still generated on the glass cover and it will slowly heat up the photovoltaic panel. Therefore, a tube that carries coolant is placed directly underneath the PV panel and an absorber plate so that heat generated is able to be absorbed into the coolant, preheating the water in the process, before transferring the preheated liquid away from the photovoltaic panel which ultimately increase the performance of a photovoltaic panel. As for the ST collector, it will collects heat when absorbing the solar radiation. Combining the preheated liquid that enters the ST collector from the PVT collector, the liquid coming out from the ST collector will have a much higher temperature since it is reheated again inside the ST collector.

The outlet tube from ST collector will enter a valve, controlled by a differential controller. This controller will be able to control the path of water flow which splits into two separate junctions based on the temperature difference between the tank and water inside the tube. If the temperature of water inside the hot water storage tank is yet to meet the required demand, the valve will allow the hot water from ST collector to enter the water storage tank. This caused the water inside the tank to increase its temperature further, reducing the temperature of cooling fluid returning to the collector simultaneously. The coolant is pump back into the collector to be reused for the next cycle.

For the second junction, the valve will only allow the coolant to pass through this junction when the hot water storage tank meets the temperature demand. This will allow the water to enter another subsystem instead of continuously supplying heat into the water storage tank. The second subsystem is also known as absorption refrigeration system, where heat from the collectors are being input into a generator consisting ammonium hydroxide. The remaining cycle involves in the transport of pure ammonia, passing through condenser, evaporator and absorber before returning to the generator again. The returning coolant is then joined with the coolant tube from the first junction before it is pump back into the collector. A clearer illustration is shown in Figure 3.3.
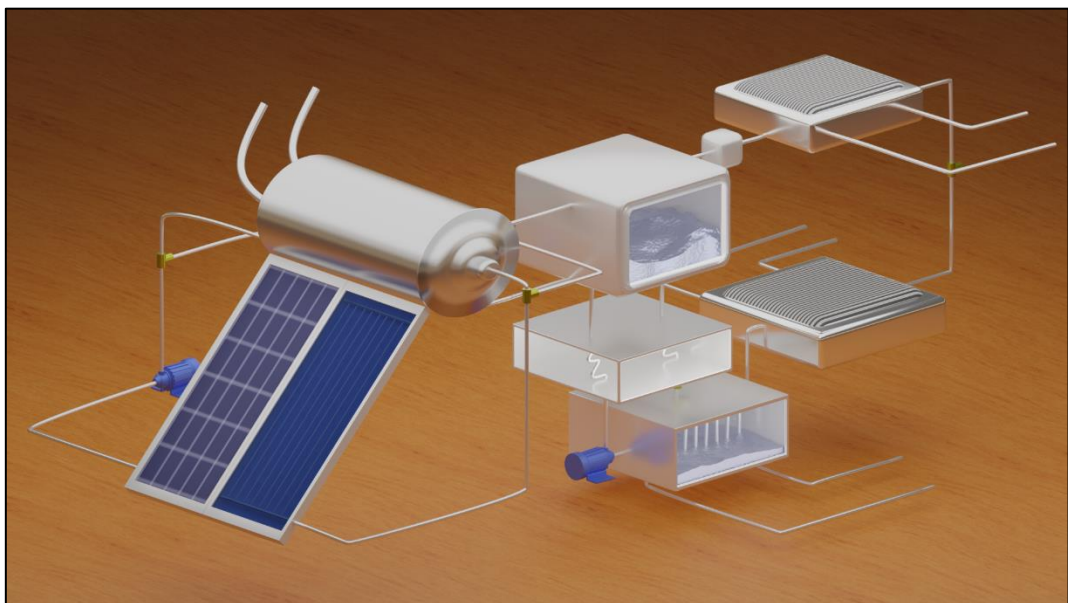
Figure 3.3: 3D model on the hybrid photovoltaic systems.

3.2.2 Design of Photovoltaic Thermal Collector and Solar Thermal Collector

The photovoltaic thermal collector and solar thermal collector are both chosen to be glazed since it has the best performance for energy and exergy efficiency. A 3 mm thick of glass cover is placed on top of each collector. Below the glass panel, there is an air gap with a thickness of 2.5 mm, for the purpose of cooling the photovoltaic cells via free convection of air. Monocrystalline silicon is chosen despite the fact that HIT-PV produced a better electrical output. This is because the probability of overheating for HIT-PV is higher. A thickness of 6 mm monocrystalline lies on top of a 0.3 mm absorber plate. The water channel consists of 8 tubes, placed below the thin absorber plate, for the purpose of transferring heat away from the collectors. Underneath the water tubes, an insulation layer with thickness of 35 mm is applied. The dimension of the PVT collector is 1.06 m x 2.018 m for the length and width, same goes to the ST collector. The only difference between both of these collectors are the additional layer present in PVT collector. With the monocrystalline layer exluded, the ST collector is thinner by 6 mm. Figure 3.4 shows the structure of the PVT collector, while Figure 3.5 shows the structure of the ST collector.
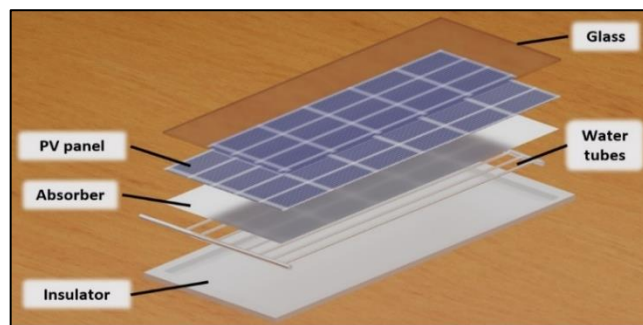
Figure 3.4: Proposed PVT collector design.
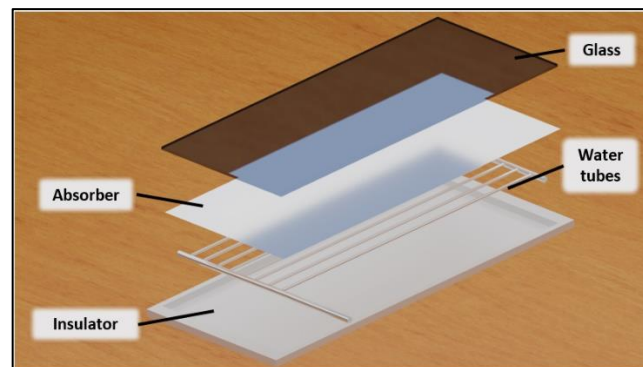
Figure 3.5: Proposed ST collector design.

The collectors will be subjected to heat loss from top, both sides, the the bottom section at the same time. Therefore, it is important to calculate the total amount of heat loss through each sections using the formula provided by Agbo and Okoroigwe (2007), in order to obtain an accurate rate of heat gained by the collector. The bottom loss coefficient can be calculated by applying equation (3.1).

$$U_b = \frac{k}{\delta_b} \qquad (3.1)$$

Where

k = thermal conductivity, W/m.K

δ_b = thickness of the bottom layer, m

Bottom loss coefficient of solar collector:

$$U_b = \frac{k}{\delta_b}$$

$$U_b = \frac{0.026 \, W/m.K}{0.035 \, m}$$

$$U_b = 0.7429 \, W/m^2.K$$

In order to calculate the side loss coefficient, every dimensions of the collectors must be known. The length, width and the total height of collectors are based on the collectors design proposed. The height of the photovoltaic thermal collector casing is 0.0968 m, while the thickness of the side casing to the middle of the absorber plate is half the length. The side loss coefficient can be calculated by applying equation (3.2).

$$U_s = \frac{2 \times L_3 \times (L_1 + L_2)}{L_1 \times L_2} \times \frac{k}{\delta_s} \qquad (3.2)$$

Where

k = Thermal conductivity, W/m.K

δ_s = Thickness of the side layer, m

L_1 = length of casing, m

L_2 = width of casing, m

L_3 = height of casing, m

Side loss coefficient of solar collector:

$$U_s = \frac{2 \times L_3 \times (L_1 + L_2)}{L_1 \times L_2} \times \frac{k}{\delta_s}$$

$$U_s = \frac{2 \times (0.0968\ m) \times (1.06\ m + 2.018\ m)}{1.06\ m \times 2.018\ m} \times \frac{0.026\ W/m.K}{0.53\ m}$$

$$U_s = 0.01367\ W/m^2.K$$

The calculation for top loss coefficient is more complex as it requires the consideration of convective heat transfer by the wind, which is denoted as α_a. Apart from finding this convective heat transfer coefficient, three more coefficients must be determined which is denoted by e, C and f. The formula for calculating the convective heat transfer coefficient and the remaining three coefficients are shown from equation (3.3) to equation (3.6). Equation (3.7) shows the formula used to calculate the top loss coefficient of solar collector.

$$\alpha_a = 5.7 + 3.8V_{wind} \tag{3.3}$$

$$e = 0.43 \left(1 - \frac{100}{T_m}\right) \tag{3.4}$$

$$C = 520(1 - 0.000051\beta^2) \tag{3.5}$$

$$f = (1 + 0.089\alpha_a - 0.1166\alpha_a\varepsilon_p)(1 + 0.07866N) \tag{3.6}$$

$$U_t = \left[\frac{N}{\frac{C}{T_m} \times \left(\frac{T_m - T_a}{N+f}\right)^e} + \frac{1}{\alpha_a}\right]^{-1} + \left[\frac{\sigma(T_m^2 + T_a^2)(T_m + T_a)}{\frac{1}{\varepsilon_p + 0.00591 \times N \times \alpha_a} + \frac{2N + f - 1 + 0.133\varepsilon_p}{\varepsilon_g} - N}\right] \tag{3.7}$$

Where

V_{wind} = wind velocity, m/s

β = tilt angle of collector, °

α_a = convective heat transfer coefficient, W/m^2.K

ε_g = glass surface emissivity

ε_p = absorber plate emissivity

σ = Stefan Boltzmann's constant, W/m^2.K^4

N = number of glass layer

T_m = mean plate temperature of absorber, K

T_a = ambient temperature, K

Side loss coefficient of solar collector:

$$\alpha_a = 5.7 + 3.8V_{wind}$$

$$\alpha_a = 5.7 + 3.8 \times (2.7778 \ m/s)$$

$$\alpha_a = 16.256 \ \text{W/m}^2.\text{K}$$

$$e = 0.43 \left(1 - \frac{100}{T_m}\right)$$

$$e = 0.43 \left(1 - \frac{100}{323 \ K}\right)$$

$$e = 0.29687$$

$$C = 520(1 - 0.000051\beta^2)$$

$$C = 520(1 - 0.000051(45°)^2)$$

$$C = 466.297$$

$$f = (1 + 0.089\alpha_a - 0.1166\alpha_a\varepsilon_p)(1 + 0.07866N)$$

$$f = \left(1 + 0.089(16.256) - 0.1166(16.256)(0.95)\right)(1 + 0.07866)$$

$$f = 0.69694$$

$$U_t = \left[\frac{1}{\frac{466.297}{323} \times \left(\frac{323-297}{1+0.69694}\right)^{0.29687}} + \frac{1}{16.256}\right]^{-1} + \left[\frac{5.7 \times 10^{-8}(323^2 + 297^2)(323 + 297)}{\frac{1}{0.95 + 0.00591 \times 1 \times 16.256} + \frac{2 + 0.69694 - 1 + 0.133(0.95)}{0.9} - 1}\right]$$

$$U_t = 6.12095 \ W/m^2.K$$

All the loss coefficients are added together to obtain the total heat loss coefficient, which is denoted by U_L. The total rate of heat loss by the solar collector can be calculated using equation (3.8).

$$\dot{Q}_L = U_L \times A \times (T_m - T_a) \tag{3.8}$$

Where

U_L = total heat loss coefficient, W/m^2.K

A = area of absorber plate, m^2

T_m = mean plate temperature of absorber, K

T_a = ambient temperature, K

Total heat loss coefficient:

$U_L = U_t + U_s + U_b$

$U_L = 6.12095\,W/m^2.K + 0.01367\,W/m^2.K + 0.7429\,W/m^2.K$

$U_L = 6.87748\,W/m^2.K$

Rate of heat loss:

$\dot{Q}_L = U_L \times A \times (T_m - T_a)$

$\dot{Q}_L = 6.87748\,W/m^2.K \times 1.873\,m^2 \times (323\,K - 297\,K)$

$\dot{Q}_L = 334.92\,W$

As for the rate of heat collected by the solar collector, the solar transmittance of the glass panel and the absorber plate must be known beforehand. The transmissivity of glass panel used in the current design is 0.9 while the absorber plate used is 0.95. The rate of heat collected by solar collector can then be calculated by applying equation (3.9).

$$\dot{Q}_u = \left(S \times \varepsilon_p \times \varepsilon_g \times A\right) - \dot{Q}_L \tag{3.9}$$

Where

S = solar irradiance, W/m^2

ε_p = transmissivity of absorber plate

ε_g = transmissivity of glass panel

A = area of absorber plate, m^2

$\dot{Q}_L$ = total rate of heat loss by collector, W

Rate of heat collected by the solar collector:

$\dot{Q}_u = \left(S \times \varepsilon_p \times \varepsilon_g \times A\right) - Q_L$

$\dot{Q}_u = (606.7\,W/m^2 \times 0.95 \times 0.9 \times 1.873\,m^2) - 334.919\,W$

$\dot{Q}_u = 636.66\,W$

Since the absorber area for both collectors are equal, they will have the same amount of heat collected. The temperature difference between the outlet temperature of the photovoltaic thermal collector and the inlet temperature and also between the outlet temperature of the solar thermal collector and the inlet temperature can then be calculated using equation (3.10).

$$\Delta T = \frac{\dot{Q_u}}{\dot{m}C_p}$$
(3.10)

Where

$\dot{Q_u}$ = rate of heat collected by the collector, W

$\dot{m}$ = water mass flow rate inside tubes, kg/s

C_p = specific heat capacity of water, kJ/kg.K

The outlet temperature of PVT collector:

$\Delta T = \dfrac{\dot{Q_u}}{\dot{m}C_p}$

$\Delta T = \dfrac{636.659\ W}{(0.016388\ kg/s)(4200\ J/kg.°C)}$

$\Delta T = 9.2\ °C$

Assuming the inlet temperature is kept at $30\ °C$,

$\Delta T = T_2 - T_1$

$T_2 = T_1 + \Delta T$

$T_2 = 30\ °C + 9.2\ °C$

$T_2 = 39.2\ °C$

The outlet temperature of ST collector:

$\Delta T = T_3 - T_2$

$T_3 = T_2 + \Delta T$

$T_3 = 39.2\ °C + 9.2\ °C$

$T_3 = 48.4\ °C$

The water from the photovoltaic thermal collector were heated from 30 °C to 39.2 °C at a solar irradiance of 606.7 W/m². After a second reheat via solar thermal collector, the outlet water temperature increased to 48.4 °C. The water will enter the hot water storage tank at this temperature to have any further heat exchange with the water inside the tank. Since both photovoltaic thermal collector and solar thermal collector have similar design, the collector efficiency is the same for both of these collectors. In order to determine the collector efficiency, the removal factor of either one of the collector must be known. Removal factor can be known as the ratio of the rate of heat collected by the collector at specific time to the maximum rate of heat collected. The maximum rate of heat collected by the solar thermal collector is obtained when the mean absorber plate temperature is at the inlet temperature of the collector. At this temperature, the rate of heat loss by collector will have the lowest value. Using equation (3.8) and equation (3.9) to obtain the maximum rate of heat collected to be 775.14 W. This result in the removal factor to be 0.82139. The collector efficiency can be calculated by applying equation (3.11).

$$\eta = (F_R \times \varepsilon_p \times \varepsilon_g) - \left(F_R \times U_L \times \left(\frac{T_2 - T_a}{S}\right)\right) \tag{3.11}$$

Where

F_R = removal factor

ε_p = transmissivity of absorber plate

ε_g = transmissivity of glass panel

S = solar irradiance, W/m²

U_L = total heat loss coefficient, W/m².K

T_2 = outlet water temperature from collector, K

T_a = ambient temperature, K

ST and PVT collector efficiency:

$$\eta = (F_R \times \varepsilon_p \times \varepsilon_g) - \left(F_R \times U_L \times \left(\frac{T_2 - T_a}{S}\right)\right)$$

$$\eta = (0.82139 \times 0.95 \times 0.9) - \left(0.82139 \times 6.87748 \, W/m^2.K \times \left(\frac{312.25 \, K - 297 \, K}{606.7 \, W/m^2}\right)\right)$$

$$\eta = 0.5602$$

3.2.3   Design of Hot Water Storage Tank

The volume of hot water storage tank that is recommended for a household with 8 people is at least 300 liters. Therefore, the chosen hot water storage tank is manufactured by Summer Solar Technology Malaysia, which has a diameter of 0.51 m, a length of 2.29 m and width of 2.43 m. The mass of an empty tank is stated to be 147 kg, while a full tank has a mass of 461 kg. This makes the total mass of water stored to be 314 kg. At any point of the day when the temperature of water inside the tank is too low even after heat exchange, a preinstalled 3 kW heating element, also known as an electric booster, is able to provide additional heating when necessary. Figure 3.6 shows the overall design of the hot water storage tank.
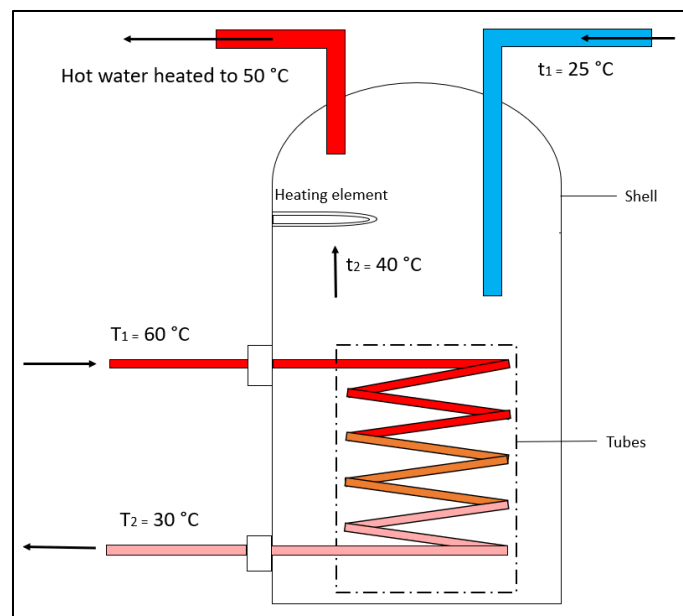
Figure 3.6: Design of the hot water storage tank at specific temperature.

Water channel exiting the solar collector will enters a hot water storage tank. It will then undergo a heat transfer with the water inside the tank, where this channel will act as a tube while the tank acts as a shell. Due to the inconsistent temperature output of water from the solar collector, a specific temperature is selected before designing the heat exchanger inside the water storage tank. By assuming the outlet temperature of water from the solar collector to be 60 °C, then decreased to 30 °C after heat exchange, input water temperature of cold water to tank at ambient temperature, and the temperature of water inside the tank after heat exchange to be 40 °C, the logarithmic mean temperature difference can be calculated using equation (3.12).

$$LMTD = \frac{(T_1 - t_2) - (T_2 - t_1)}{\ln \left[\frac{(T_1 - t_2)}{(T_2 - t_1)}\right]} \tag{3.12}$$

Where

T_1 = inlet tube temperature, K

T_2 = outlet tube temperature, K

t_1 = inlet temperauture of shell, K

t_2 = outlet temperature of shell, K

Calculating the logarithmic mean temperature difference:

$$LMTD = \frac{(T_1 - t_2) - (T_2 - t_1)}{\ln \left[\frac{(T_1 - t_2)}{(T_2 - t_1)}\right]}$$

$$LMTD = \frac{(60\,°C - 40\,°C) - (30\,°C - 25\,°C)}{\ln \left[\frac{(60\,°C - 40\,°C)}{(30\,°C - 25\,°C)}\right]}$$

$$LMTD = 10.82021\ K$$

According to requirement stated by United States Environmental Proctection Agency (2020), the maximum mass flow rate for shower is set to be approximately 0.125 kg/s for every household water supply. With the mass flow rate known, the rate of heat transfer can be obtained by using equation (3.13).

$$\dot{Q} = \dot{m}C_p\Delta T \tag{3.13}$$

Where

$\dot{m}$ = mass flow rate of water,

C_p = specific heat capacity of water, kJ/kg.K

ΔT = temperature difference between the inlet and outlet, K

Rate of heat transfer inside hot water tank:

$$\dot{Q} = \dot{m}Cp\Delta T$$

$$\dot{Q} = 0.125\ kg/s \times 4.2\ kJ/kg.K \times (40\,°C - 25\,°C)$$

$$\dot{Q} = 7.88\ kW$$

Using the results obtained, the area of heat transfer can be calculated by applying equation (3.14). The overall heat transfer coefficient used is 397.5 W/m^2.K, where both fluid content is water through a copper tube. (Engineering ToolBox, 2003)

$$\dot{Q} \ = \ U \times A \times \ LMTD \tag{3.14}$$

Where

U = overall heat transfer coefficient, W/m^2.K

A = area of heat transfer, m^2

$LMTD$ = logarithmic mean temperature difference, K

Calculating the heat transfer area:

$\dot{Q} \ = \ U \times A \times LMTD$

$A \ = \ \dfrac{\dot{Q}}{U \times LMTD}$

$A \ = \ \dfrac{7.875 \ kW}{397.5 \ W/m^2.K \times 10.82021 \ K}$

$A \ = \ 1.830955 \ m^2$

EnggCyclopedia (2020) have stated the methods of calculating the tube velocity and Reynolds number of flow. With the amount of heat transfer area obtained, total number of tubes inside heat exchanger can first be obtained using equation (3.15).

$$n_t \ = \ \frac{A}{\pi \times D_o \times L} \tag{3.15}$$

Where

A = heat transfer area, m^2

D_o = outer diameter of tubes, m

L = length of tube

The outer diameter of tubes are chosen from the standard size, which is 1.9 inches or approximately 0.04826 mm. The total length of tubes inside the heat exchanger is 18 feet, which is approximately 5.4864 m.

Number of tubes inside heat exchanger:

$$n_t = \frac{1.830955 \ m^2}{\pi \times 0.04826 \ m \times 5.4864 \ m}$$

$$n_t = 2.201232 \approx 2 \ tubes$$

Based on the property of the chosen solar collectors, the volumetric flow rate is 0.000017 m³/s. Simply dividing the volumetric flow rate with the specific volume at 60 °C, which is 0.001017 kg/s, will obtain a mass flow rate of 0.01638 kg/s. The tube velocity can then be calculated by applying equation (3.16).

$$V_t = \frac{4\dot{m}(N_p/N_t)}{\pi \times \rho \times D_i^2} \qquad (3.16)$$

Where

$\dot{m}$ = mass flow rate of tube fluid, kg/s

N_p = number of tube pass

N_t = number of tubes

D_i = inner diameter of tubes, m

ρ = density of tube fluid, kg/m³

For a tube with an outer diameter of 0.04826 m, the inner diameter is approximately 0.0381 mm. Since water is selected as the medium of heat transfer, the density of water at 60 °C is 983.2 kg/m³ (Çengel, Boles and Kanoglu, 2020). A 10 tube pass configuration is selected for the purpose of higher heat exchange rate.

The tube velocity:

$$V_t = \frac{4\dot{m}(N_p/N_t)}{\pi \times \rho \times D_i^2}$$

$$V_t = \frac{4 \times (0.01639 \ kg/s)(10 \ tube \ pass \ / \ 2 \ tubes \ )}{\pi \times (983.2 \ kg/m^3) \times (0.0381 \ m)^2}$$

$$V_t = 0.0731 \ m/s$$

The rate of heat transfer is higher if the fluid flow is turbulent. The higher the Reynolds number will result in better heat exchange rate. The Reynolds number of the tube fluid content can then be calculated using equation (3.17).

$$V_t \ = \ \frac{4\dot{m}(N_p/N_t)}{\pi \times \mu \times D_i} \tag{3.17}$$

Where
$\dot{m}$ = mass flow rate of tube fluid, kg/s
N_p = number of tube pass
N_t = number of tubes
D_i = inner diameter of tubes, m
μ = dynamic viscosity, Pa.s

The dynamic viscosity of water at 60 °C is 0.000469 Pa.s, which can be obtained from Engineers Edge (2014). The remaining parameters are similar to the parameters used in equation (3.16).

The Reynolds number:

$$Re \ = \ \frac{4\dot{m}(N_p/N_t)}{\pi \times \mu \times D_i}$$

$$Re \ = \ \frac{4 \times (0.01639 \ kg/s)(10 \ tube \ pass \ / \ 2 \ tubes \ )}{\pi \times (0.00047 \ Pa.s) \times (0.0381 \ m)}$$

$$Re \ = \ 5838.8 \ (Turbulent)$$

In order to check whether there is enough space to install the heating coil inside the hot water storage tank, the surface area of the tank has to be known. Using the dimensions specified earlier, while assuming that the tank is a perfect cylinder, the surface area obtained is approximately 4.07751 m^2. Dividing the heat transfer area with the surface area obtained will result in getting the percentage of area occupied. The percentage obtained is 44.9037%, which means that the heat exchanger section occupies less than half of the tank.

3.2.4   The Absorption Refrigeration System

The absorption refrigeration system implemented into the design is an additional application that is able to utilize the remaining heat collected from both solar collectors. Since it is not required to have anymore production of hot water for shower once the hot water have reached its peak temperature, the excessive hot water is transferred away into an absorption refrigeration system mainly for space cooling. The refrigerant used in this system is pure ammonia, which is first in the form of rich ammonium hydroxide solution inside the generator. Hot water from the collector will have a heat exchange with the content consisting the rich ammonium hydroxide solution. Due to the low boiling point of ammonium hydroxide, which is merely 37.7 °C, ammonium hydroxide with temperature that exceeds the boiling point will cause it to boil. Once boiled, pure ammonia will escape the generator and becomes the heat transfer medium. To prevent any water vapour from escaping with the escaped ammonia, a rectifier is used to only allow pure ammonia to pass through. This is achieved by cooling the escaped mixture containing water vapour and ammonia which then allows the water vapour to condense into water. Water will then returned to the generator to be mixed with the ammonium hydroxide solution again. The pure ammonia vapour will be condensed and have lower pressure once it passes the condenser and expansion valve. The ammonia then enters the evaporator, where heat exchange between the ammonia tube and air channel occurs. It is able to cool off the air to a lower temperature. In the same time, the liquid ammonia gains heat and is able to change to ammonia vapour before entering the absorber. The ammonium hydroxide inside the absorber was initially a weak solution. When the ammonia vapour enters the absorber, it is absorbed by the weak ammonium hydroxide solution. This will result in obtaining rich ammonium hydroxide solution that is ready to be pumped into the generator. A regenerator is installed between the absorber and generator mainly for the purpose of transferring excess heat into the rich ammonia vapour that was pumped back into the generator.

3.2.5 Design of Evaporator in Absorption Refrigeration System

By looking solely on the evaporator section, the exit velocity of the air produced for space cooling can be calculated in order to check the reliability of the absorption refrigeration system. The mass flow rate of dry air and water vapour is also essential in order to design the heat exchanger inside the evaporator. However, it is difficult to determine every temperature at different point inside this subsystem. Therefore, the calculation is carried out with the system been fixed at one temperature. The design proposed is shown in Figure 3.7.
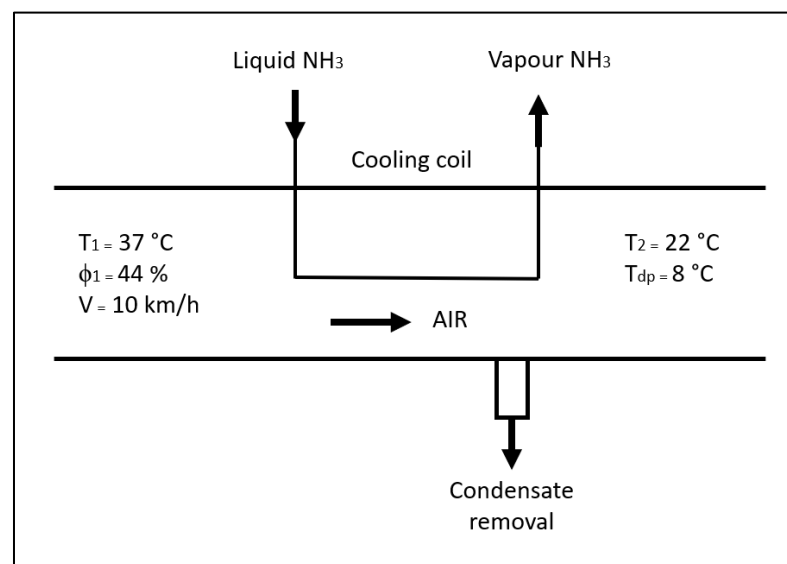
Figure 3.7: Design of the evaporator at specific temperature.

The temperature entering the air ducting is set to be according to the dry bulb temperature, which is 37 °C. The relative humidity is 0.44, and the velocity is set to 10 km/h. After air has passed through the cooling coil, the outlet dry bulb temperature will be decreased to 22 °C, with a dew point of 8 °C. The radius of the air ducting is set to be 40 cm. For the system at one atmospheric pressure, pychrometric chart can be used to determine the specific humidity, enthalpy and also the specific volume for the inlet and outlet air. The result extracted from the chart will be shown in Figure A-1 and Figure A-2 from appendix. Inlet enthalpy is 82 kJ/kg dry air, specific humidity of inlet is 0.0175 kg water/kg dry air, specific volume of inlet is 0.92 m^3/kg dry air, outlet enthalpy is 39.5 kJ/kg dry air, specific humidity of outlet is 0.0065 kg water/kg dry air, specific volume of outlet is 0.844 m^3/kg dry air. The outlet humidity ratio is calculated by dividing the outlet pressure at dew point with the outlet pressure at dry

bulb temperature. Outlet pressure at dew point is 1.08586 kPa while the outlet pressure at dry bulb temperature is 2.67144 kPa The relative humidity is calculated to be 0.40647.

With the inlet velocity known, the volumetric flow rate can be calculated by multiplying its velocity with the cross sectional area of the air ducting. Since the radius of the air ducting is set to 40 cm, the cross sectional area is 0.12566 m^2. Therefore, the volumetric flow rate is calculated to be 0.34906 m^3/s. Dividing the volumetric flow rate with the inlet specific volume will result in obtaining the mass flow rate of dry air, which is 0.37941 kg/s. Applying the water mass balance to obtain the mass flow rate of water vapour, which is shown in equation (3.18).

$$\dot{m}_w = \dot{m}_a(\omega_1 - \omega_2) \tag{3.18}$$

Where

$\dot{m}_a$ = mass flow rate of dry air, kg/s

ω_1 = inlet specific humidity, kg water/kg dry air

ω_2 = outlet specific humidity, kg water/kg dry air

Water mass balance:

$$\sum \dot{m}_{w,i} = \sum \dot{m}_{w,e}$$

$$\dot{m}_{a1}\omega_1 = \dot{m}_{a2}\omega_2 + \dot{m}_w$$

$$Since\ \dot{m}_{a1} = \dot{m}_{a2} = \dot{m}_a$$

$$\dot{m}_w = \dot{m}_a(\omega_1 - \omega_2)$$

$$\dot{m}_w = 0.37941\ kg/s \times (0.0175 - 0.0065)\ kg\ water/kg\ dry\ air$$

$$\dot{m}_w = 0.00417\ kg/s$$

The energy balance on control volume is used in order to calculate the total rate of heat transfer inside the evaporator. The enthalpy of water vapour is according to the outlet dry bulb temperature, which is 92.281 kJ/kg and is obtained from the table provided by Çengel, Boles and Kanoglu (2020). The formula to find the rate of heat transfer for evaporator is shown in equation (3.19).

$$\dot{Q}_{out} = \dot{m}_a(h_1 - h_2) - \dot{m}_w h_{w2} \tag{3.19}$$

Where

$\dot{m}_a$ = mass flow rate of dry air, kg/s

$\dot{m}_w$ = mass flow rate of water vapour, kg/s

h_1 = inlet enthalpy of dry air, kJ/kg

h_2 = outlet enthalpy of dry air, kJ/kg

h_w = enthalpy of water vapour, kJ/kg

Energy balance on control volume:

$h_{w2} = h_{f@22\,°C} = 92.281 \, kJ/kg$

$\dot{E}_{in} - \dot{E}_{out} = 0$

$$\sum \dot{m}_i h_i = \sum \dot{m}_e h_e + \dot{Q}_{out}$$

$\dot{Q}_{out} = \dot{m}_a(h_1 - h_2) - \dot{m}_w h_{w2}$

$\dot{Q}_{out} = (0.37941 \, kg/s)(82 - 39.5) \, kJ/kg - (0.00417 \, kg/s)(92.281 \, kJ/kg)$

$\dot{Q}_{out} = 15.74 \, kW$

By multiplying the outlet specific volume with the mass flow rate of dry air, the outlet volumetric flow rate of air can be calculated to be 0.32022 m³/s. As for the velocity of outlet air, it can be calculated by simply dividing this volumetric flow rate with the cross sectional area used for ducting. An outlet velocity of 2.54831 m/s is obtained.

In order to determine the mass flow rate of the liquid ammonia, one assumption has to be made. The obtained rate of heat transfer inside the cooling coil is assumed to be equal to the rate of heat transfer inside the air ducting without any losses. With this assumption, the mass flow rate of the liquid ammonia can be calculated by reusing the formula from equation (3.13). The specific heat capacity of ammonia used is 2.2 kJ/kg.K, and a total change of 10 °C in the evaporator coil temperature.

Due to the fact that the pressure alters with the altitude, houses at different altitude tends to have different velocity of air produced. Every data obtained from the psychrometric chart cannot be used since the chart which is previously used is only for one atmospheric pressure only. Therefore, in order to determine the enthalpy, specific humidity and specific volume, it is required to calculate each one individually.

By multiplying the relative humidity of inlet ducting with the saturation pressure at inlet dry bulb temperature, the partial pressure of water vapour at inlet of the ducting can be obtained, which is equal to 2.78586 kPa. The dew point at the inlet of the ducting is determined by the temperature which produces this amount of pressure, which is calculated to be 22.7 °C. This means that for any outlet temperature that is lower than 22.7 °C, part of the moisture will be condensed. The atmospheric air is first assumed to be ideal, with the pressure equal to the sum of partial pressure of water vapour and that of dry air. Therefore, the partial pressure of dry air can be obtained by subtracting the atmospheric pressure with the partial pressure of water vapour. As for the specific volume, it can be calculated by using equation (3.20).

$$v = \frac{RT}{P_a} \qquad (3.20)$$

Where

R = gas constant of air, kJ/kg.K

T = dry bulb temperature, K

P_a = partial pressure of dry air, kPa

The specific humidity can be calculated by using the atmospheric pressure and the partial pressure of water vapour. The formula is shown in equation (3.21).

$$\omega = \frac{0.622 \times P_v}{P_1 - P_v} \qquad (3.21)$$

Where

P_1 = atmospheric pressure, kPa

P_v = partial pressure of water vapour, kPa

The enthalpy of dry air is equal to the enthalpy of saturated vapour at dry bulb temperature. The specifc heat capacity of air used is 1.005 kJ/kg.K. Using these parameters, the enthalpy of air can be found using equation (3.22).

$$h = C_p T + \omega h_g \qquad (3.22)$$

Where

C_p = specific heat capacity of air, kJ/kg.K

T = dry bulb temperature, K

ω = specific humidity, kg water/kg dry air

h_g = enthalpy of dry air, kJ/kg dry air

For the partial pressure of outlet air, it is equivalent to the pressure at outlet dew point temperature, which is obtained to be 1.08586 kPa. The partial pressure of outlet dry air is calculated the same way as the inlet, that is to subtract the atmospheric pressure with the partial pressure of the outlet water vapour.

The specific volume, specific humidity and enthalpy of outlet air can be calculated by reapplying equation (3.20), equation (3.21) and equation (3.22) respectively.

The volumetric flow rate of inlet air remains the unchanged, which is 0.34906 m³/s. Due to the changes in specific volume, the mass flow rate of dry air alters. The theoretical value for mass flow rate of dry air can be obtained the same way, that is to divide the volumetric flow rate with the specific volume. Using the water mass balance equation from equation (3.18), the mass flow rate of water vapour can be obtained. As for the energy balance on control volume, the rate of heat transfer can be calculated by using back equation (3.19). The theoretical value of exit volumetric flow rate of air can be found by multiplying the outlet specific volume with the mass flow rate of dry air. The exit velocity and mass flow rate of refrigerant is obtained similarly to the methods previously stated. A sample calculation showing the theoretical result at 1 atmospheric pressure is shown in Appendix B-1.

At one atmospheric pressure, the theoretical value of exit velocity of air is 2.59853 m/s and the mass flow rate of refrigerant is calculated to be 1.0571 kg/s. Using the mass flow rate of refrigerant obtained, the design of heat exchanger can be done. Considering the previous assumption made, where there is no heat loss in the evaporator, the total rate of heat transfer is 16.28 kW.

Similar to the design process of the heat exchanger in the hot water storage tank, the logarithmic mean temperature difference is calculated using equation (3.12), which will be 15.6609 K. The overall heat transfer coefficient of ammonia inside evaporator is approximately 1135.65 W/m^2.K, which is obtained from Engineers Edge, L.L.C. (2021). By using equation (3.14), the area of heat transfer can be calculated to be 0.9153 m^2. Tubes have outer diameter of 0.0254 m, an internal diameter of 0.0191 m and a total length of 1.83 m. The number of tubes are then calculated to be six by using equation (3.15). Giving a total of two tube passes, the tube fluid velocity can be found. The density of liquid ammonia used is 674 kg/m^3 (Engineering ToolBox, 2018) and have a dynamic viscosity of 0.000266 Pa.s, which are obtained from Concoa (2012). The tube fluid velocity is calculated to be 1.8343 m/s with a Reynolds number of 88541.

The coefficient of performance for the absorption refrigeration system can be found by fixing the temperature of the refrigerated space. This temperature is assumed to be 10 °C. Water from the outlet of solar thermal collector will be provide heat to the ammonia water solution inside the generator. Therefore, the temperature of heat source is equal to the temperature obtained from the outlet of the solar thermal collector. With these parameters known, equation (3.23) can be applied to find the coefficient of performance.

$$COP = \left[\frac{(1-T_a)}{T_s}\right]\left[\frac{T_l}{(T_l-T_a)}\right] \tag{3.23}$$

Where

T_a = ambient temperature, K

T_s = heat source temperature, K

T_l = temperature of refrigerated space, K

CHAPTER 4

RESULTS AND DISCUSSIONS

4.1 Photovoltaic Thermal Collector and Solar Thermal Collector

4.1.1 Solar Irradiance and Ambient Temperature Throughout a Day

An approximation is used based on the position of sun in the sky throughout one year, which is obtained from PVEducation (2021). This calculation involves in the usage of latitude for the current location and also on a specific day of the year, giving results on an hourly basis. A 4° latitude is used and the date is set to 10 March 2021, with the ambient temperature following the data obtained from Timeanddate (2021). Figure 4.1 and Figure 4.2 shows the amount of solar irradiance and the ambient temperature for every hour respectively on 10 March 2021.
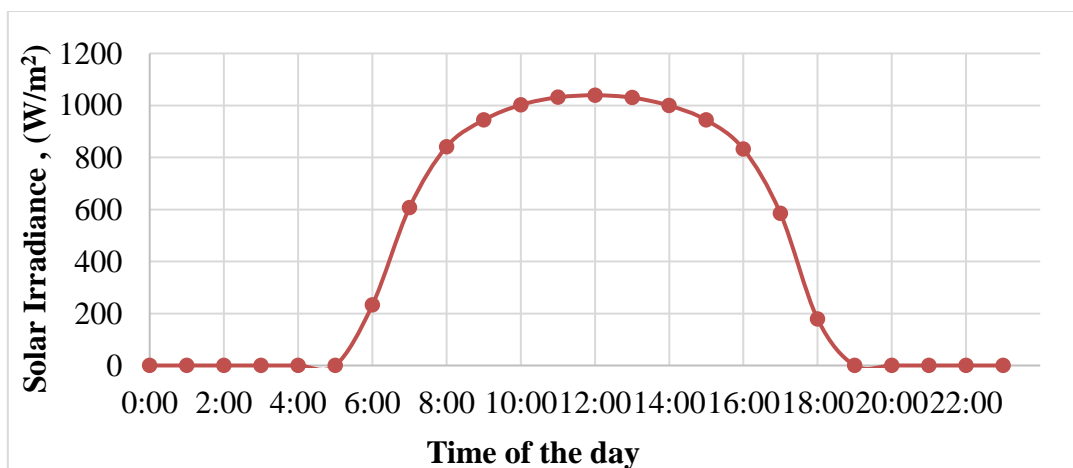
Figure 4.1: Solar irradiance throughout the day.
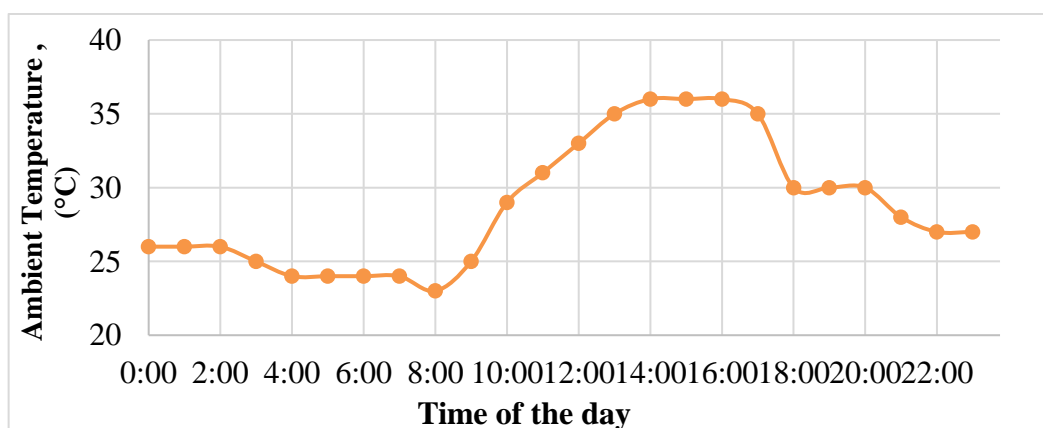
Figure 4.2: Ambient temperature throughout the day.

4.1.2 Rate of heat Collected by PVT Collector and ST Collector

Considering the fact that the solar irradiance and ambient temperature varies for every hour, the rate of heat collected changes accordingly. The rate of heat collected by both collectors is obtained by first calculating the loss coefficient by each collector. The side loss coefficient and bottom loss coefficient remains unchanged even for different ambient temperature. Not only that, the convective heat transfer coefficient together with the remaining coefficients are not affected by ambient temperature. Therefore, only equation (3.7) is used to calculate the top loss coefficient. After applying equation (3.8) to obtain the total rate of heat loss by collector, the rate of heat collected can then be calculated using equation (3.9). This calculation is repeated for every hour, with Figure 4.3 showing the rate of heat collected by a single collector in every hour.
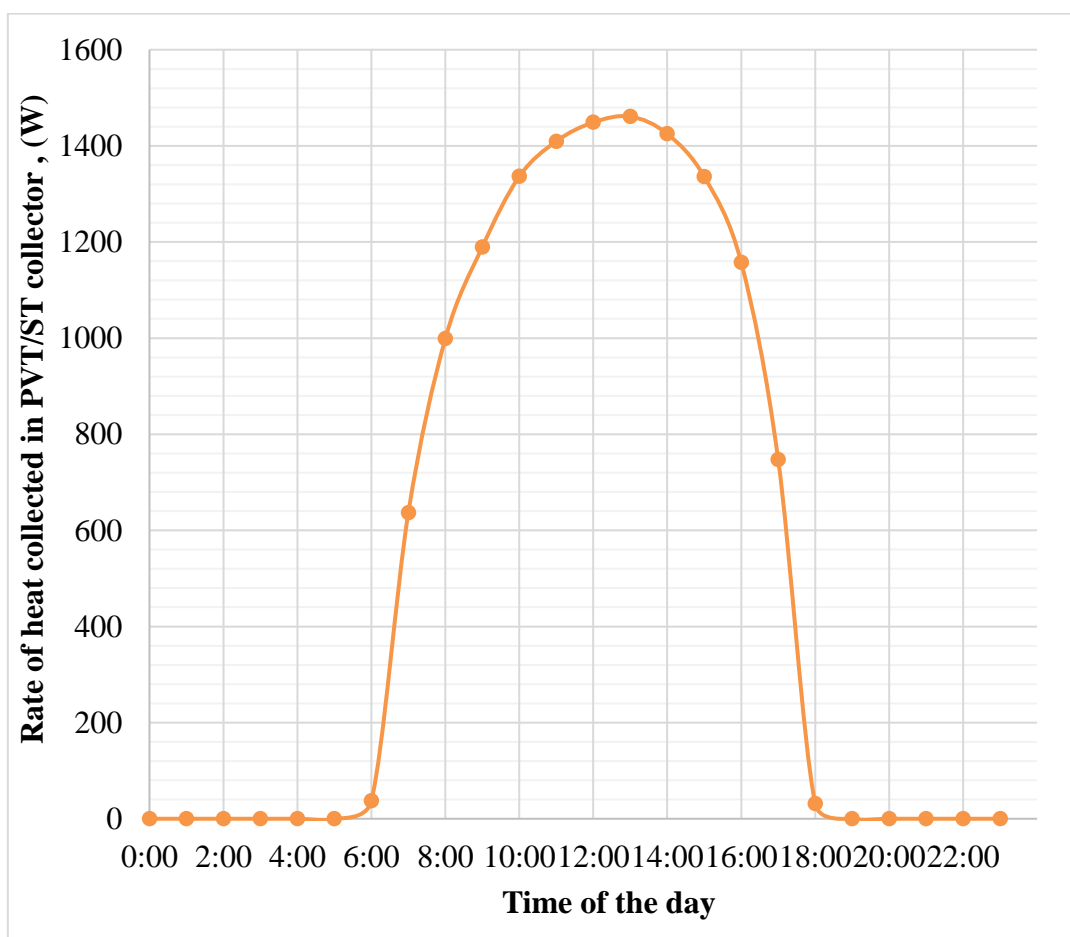
Figure 4.3: Rate of heat collected by each collector throughout the day.

4.1.3 Collector efficiency of PVT Collector and ST Collector

Similar to the rate of heat collected by the collectors, due to the various ambient temperature and solar irradiance obtained in each hour, the outlet temperature of both collectors have changed. This causes the removal factor and collector efficiency varies accordingly. Using the rate of heat collected at every hour, which is obtained in the previous section, the temperature difference between the outlet temperature and the inlet temperature of the photovoltaic thermal collector and also between the outlet temperature and the inlet temperature of the solar thermal collector can be determined. Using back equation (3.10), the temperature difference for each hour can be calculated. After obtaining the output temperature of solar thermal collector, the minimum rate of heat loss by each collector can be calculated by assuming the mean absorber plate temperature equal to the inlet collector temperature. Replacing the inlet collector temperature in equation (3.8), and using the obtained result in equation (3.9), the maximum rate of heat collected can be calculated. The removal factor can then be obtained by dividing the rate of heat collected with the maximum rate of heat collected. The collector efficiency is calculated by using equation (3.11) for every hour, with the results obtained shown in Figure 4.4.
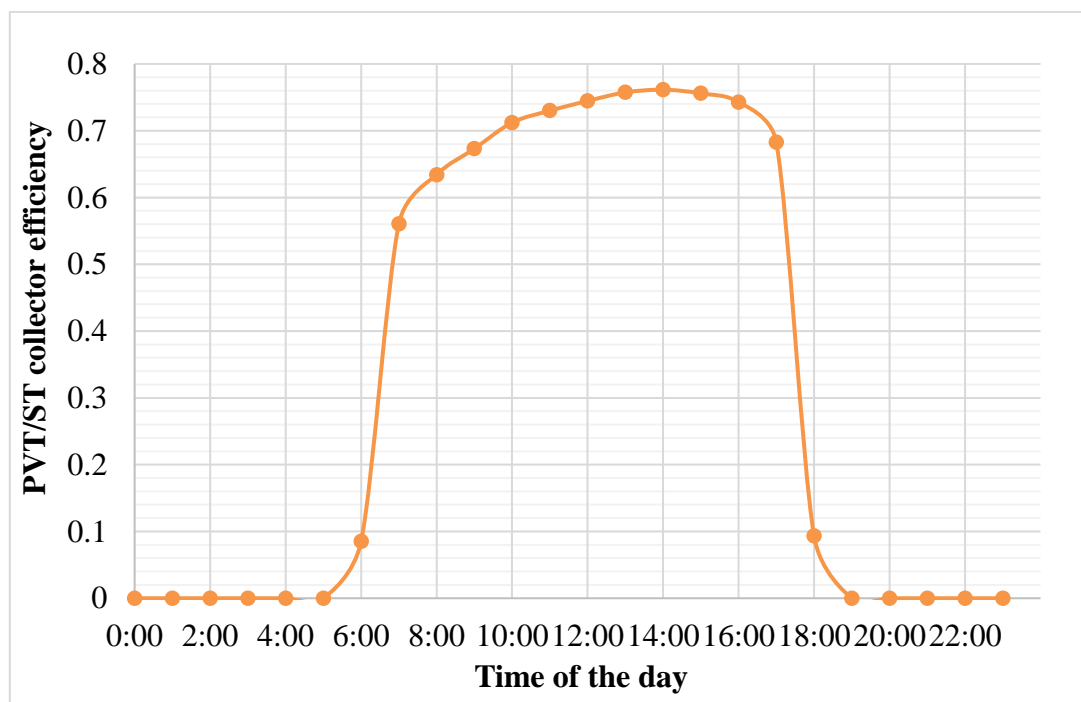
Figure 4.4: Collector efficiency throughout the day.

4.1.4 Summary on the Results Obtained for Both Collectors

From the previous two figures shown, which is Figure 4.3 and Figure 4.4, the overall trend of both graphs is quite similar. Both graphs give an obvious representation of a parabolic graph. The solar irradiance is first shone at 6:00 with a very low amount, only at 232.3 W/m^2. This result in the lowest amount of collector efficiency too, with only 0.085244. After 6:00, the solar irradiance increases tremendously until 9:00, where the solar irradiance increases at a slower rate for the next seven hours. Both the rate of heat collected and the collector efficiency have shown to have a tremendous increase at 7:00. There is only a slight difference in the solar irradiance between 10:00 to 14:00, where the results obtained follow accordingly.

There is one small difference on the time where it gives the maximum result. The peak amount of solar irradiance happens at 12:00, where a total of 1039 W/m^2 is recorded. However, the maximum rate of heat collected obtained occurs at 13:00, where it reaches up to 1460.95 W. The same goes for the collector efficiency, as the peak value obtained is occurring at 14:00, where it reaches 0.7613.

Apart from this difference, from 14:00 onwards, the trend between these three graphs is pretty much similar. The solar irradiance falls off rapidly starting from 16:00, all the way to 18:00 where it drops 178.6 W/m^2, which is consider to be a very low amount. After 18:00, since there is no amount of solar irradiance recorded, both collectors will have no heat collected and thus will have no efficiency.

The outlet temperature of solar thermal collector will be shown in later section, under the results obtained in hot water storage tank. This is because the outlet water from solar thermal collector will undergo heat exchange inside the hot water storage tank and it requires further calculation in order to determine the temperature of water inside this storage tank.

4.2   Solar Hot Water System

4.2.1   Temperature of Water inside Hot Water Storage Tank

The outlet water tubes from solar thermal collector will enter the heat exchange section inside the hot water storage tank. By fixing the dimensions and the properties of the hot water storage tank used, which has a heat transfer area of 1.9481 m^2 and consists of 2 tubes with a total of 10 tube passes, the temperature of water inside the storage tank can be determined after heat exchange. This can be done by equating equation (3.13) and equation (3.14). However, this will lead to a very complex equation to solve. Therefore, trial and error are used so that both equation will result in the same value in order to obtain the solution. An example is shown in Appendix B-2. Repeating the calculation for every temperature of the outlet of solar thermal collector obtained. The temperature of water inside the tank after heat exchange for each hour can be obtained. The result obtained is shown in Figure 4.5.
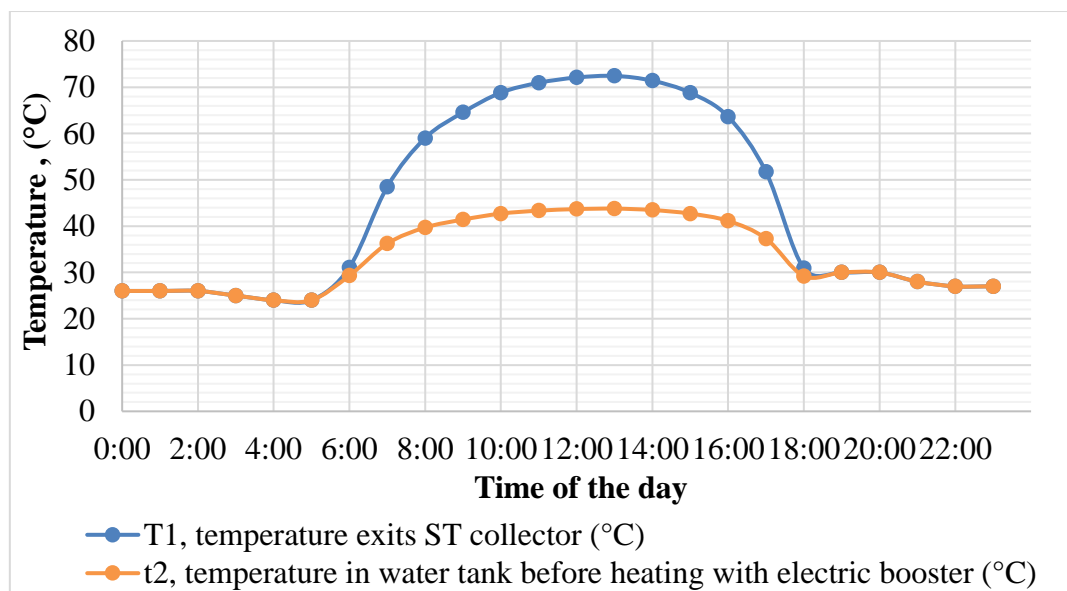
Figure 4.5: ST collector outlet temperature and water tank temperature.

From Figure 4.5, for any time without any solar irradiance, that is between 19:00 to 5:00, the outlet of ST collector will follows the ambient temperature. The same goes to the water inside the hot water storage tank since the input temperature from the faucet is according to the ambient temperature as well. Observing Figure 4.5, even after the solar thermal collector outlet temperature exceeds 75 °C, the temperature of water inside the storage tank rises by a maximum of about 19 °C only. The hottest water obtained after heat exchange is 43.8 °C, which occurs at 13:00.

4.2.2 Daily Power Usage of Electric Booster inside Hot Water Storage Tank

Before calculating for the power consumption used by the electric booster from the hot water storage tank, energy and the time required must first be obtained. With the water temperature inside storage tank obtained previously, the energy and time required for the electric booster to heat up to 50 °C can be found. This is because the standard hot shower water temperature can be up to a maximum of 50 °C. At any point of the day, using the obtained temperature of water inside the storage tank after heat exchange, a temperature difference can be calculated by subtracting 50 °C with the obtained water temperature. The energy required to heat all of the water inside the storage tank can be obtained by using equation (3.13), which the results obtained will be shown in Table C-1. Using the power and energy relation, by using the 3 kW electric booster installed, the time required for the electric booster to heat to required energy can be calculated. Figure 4.6 shows the time required to heat the water inside storage tank up to 50 °C if the electric booster is turn on for any hours throughout the day.
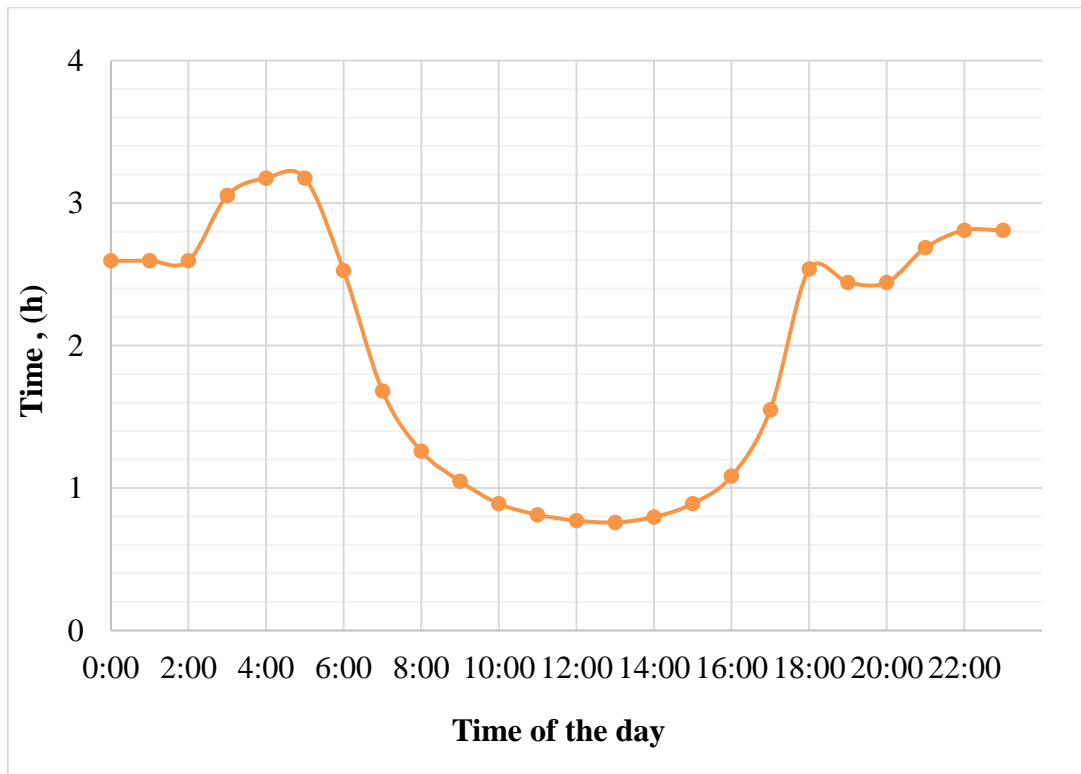
Figure 4.6: Time required for a 3kW electric booster to heat the water inside storage tank to 50 °C throughout the day.

From the results obtained in Figure 4.6, the most preferable time to turn on the electric booster to heat up to the required maximum temperature for hot shower is between 11:00 to 15:00. The least time required occurs at 13:00, where the electric booster only requires to be turned on for 0.75871 hours to produce a full tank at 50 °C. This is approximately 45 minutes. This electric booster is only required to be turned on once per day because a full tank with 300 liters is more than enough to provide water for hot shower on a household with eight people daily. However, the results obtained may not be accurate for certain times where there is a huge increase or decrease in solar irradiance. For example, the electric booster will take 2.5265 hours to increase the water temperature to 50 °C at 6:00. The solar irradiance will rise rapidly in 2.5265 hours, from 232.3 W/m^2 to 900 W/m^2. Not to mention, the ambient temperature will also increase by a slight amount. This means that the increase in ambient temperature and solar irradiance will result in greater heat exchange between the solar thermal collector and the hot water storage tank. Therefore, the required time required at these hours should be lower than the results obtained.

The amount of power used by this electric booster daily is essential in finding the overall saving in terms of electricity consumption when comparing this solar hot water system with the instant water heater system. By multiplying the time obtained previously, with the power rating of the electric booster used, the power represented by kilowatts hours can be achieved. The results will be shown in Figure 4.7.
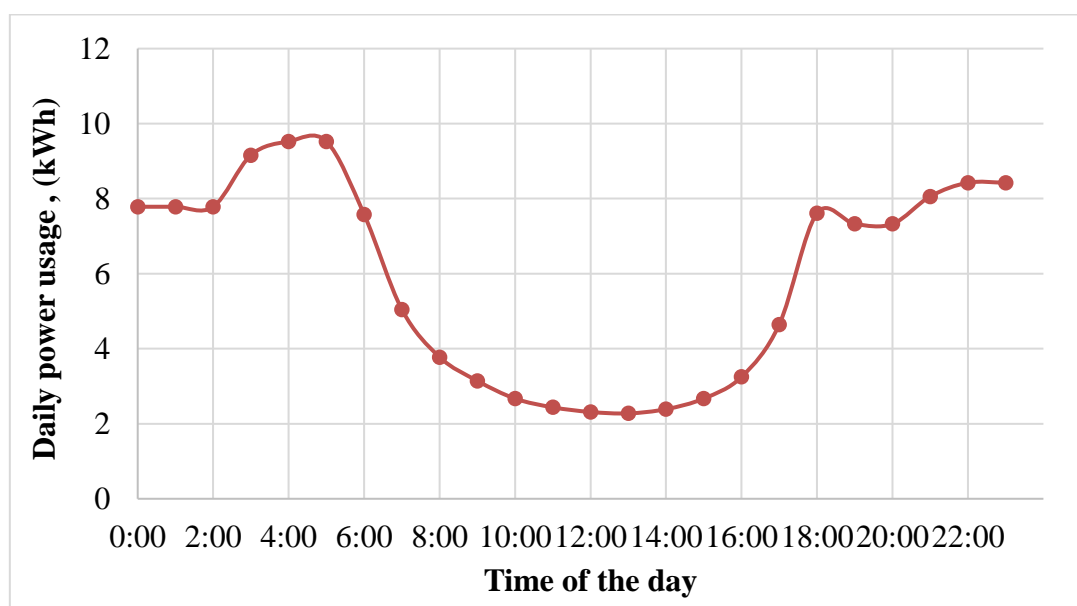
Figure 4.7: Amount of power used by electric booster if turn on at different hour.

4.2.3   Total Heat Energy Stored inside Hot Water Storage Tank

In order to know how much heat energy is stored inside the hot water storage tank, the rate of heat transfer from the heat exchanger inside the storage tank must first be known, which can be obtained by using equation (3.14). Figure 4.8 shows the obtained rate of heat transfer throughout a day.
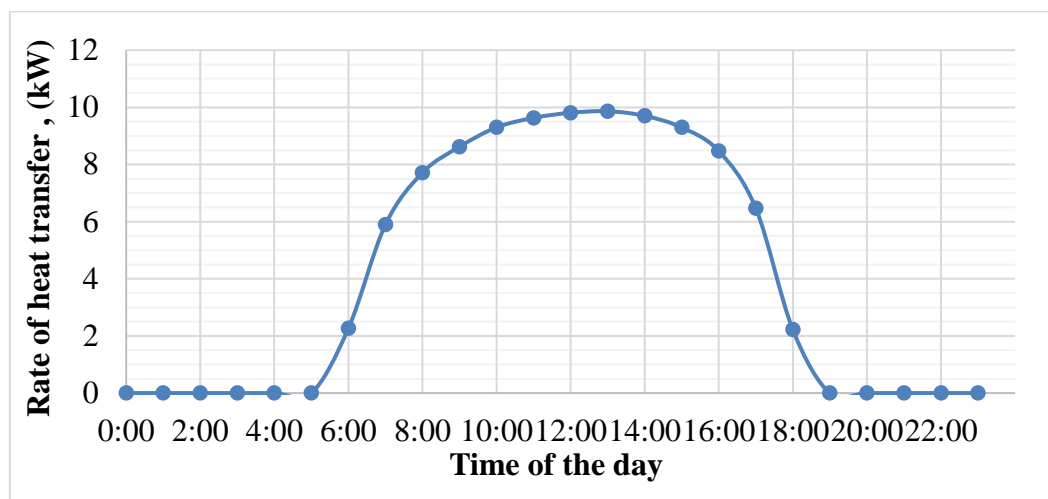
Figure 4.8: Rate of heat entering the water tank throughout the day.

The sum of area under the graph shown in Figure 4.8 will give the total amount of energy. The whole water storage tank is assumed to have little to no heat loss. This will be possible when thick layer of insulation material is applied onto the surface of the storage tank. Using the obtained energy for each hour, the cumulative energy stored in the hot water storage can be calculated by adding the the gain in energy from each hour. The cumulative energy of the hot water storage tank is shown in Figure 4.9.
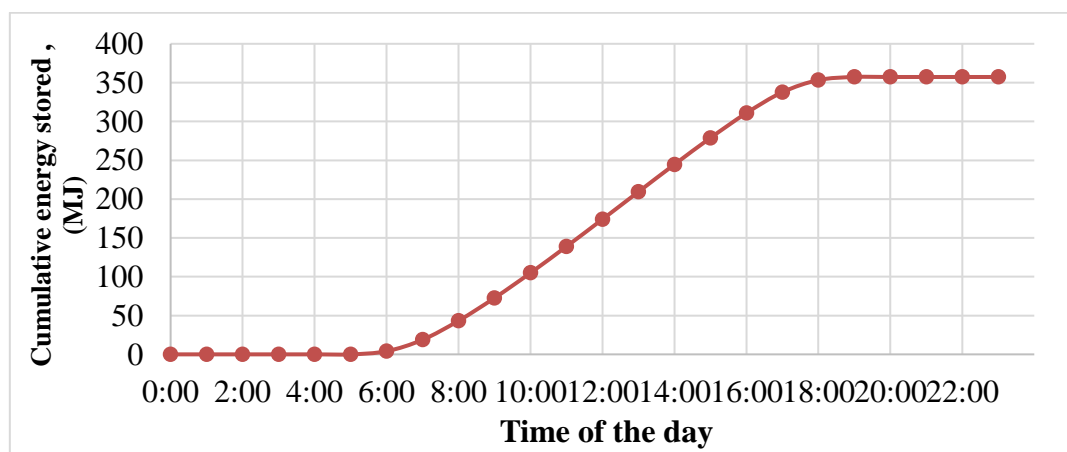
Figure 4.9: Cumulative energy stored in storage tank throughout the day.

4.2.4   Additional Note on The Availability of Hot Water Produced

The size of the hot water storage tank used can provide hot water shower up to eight people. This means that for any household with smaller size, the remaining water which is left unused is able to reserve for the next day, saving the needs for electric booster to function. There is little to no concern on the temperature of water dropping significantly over the next day as the whole storage tank is applied with a thick layer of insulation, which can cut the heat loss by up to 45%.

Another factor is on the mass flow rate used by shower. The mass flow rate used in the previous calculation is following the maximum mass flow rate stated by United States Environmental Proctection Agency. By using a lower mass flow rate of hot water supplied, and repeating the calculation by equating equation (3.13) and equation (3.14), the temperature of water inside the storage tank will be higher after the heat exchange with the outlet solar thermal collector. A sample of this calculation can be found in Appendix B-3. With the temperature of water inside storage tank being higher, no additional heating is required provided that the required hot shower temperature is met. This may ended up reducing the total electricity consumption as there is no work on the electric booster.

Using the previous point on the effect of mass flow rate, the design of the hot water storage tank can be modified so that the mass flow rate of water during heat exchange is independent to the output usage of hot water. The mass flow rate of water during heat exchange can be set lower so that there is higher rate of heat exchange. When heat exchange is no longer necessary, the water can be pumped so that the required mass flow rate can be achieved. This will also allows more time for the hot water to operate the absorption refrigeration system since the time required to heat up the hot water storage tank is shorter with lower mass flow rate.

4.3   Absorption Refrigeration System

4.3.1   Results Obtained at Different Pressure for Space Cooling

Since pressure alters with the altitude, results obtained for different altitude tends to vary. Therefore, each pressure input has to be calculated individually to determine the enthalpy, specific humidity and specific volume before calculating for the velocity of outlet air. As for the heat exchanger section inside the evaporator, the rate of heat transfer will change with increasing pressure. The input pressure is ranging from 70 kPa to 101.3 kPa. The results obtained for the logarithmic mean temperature difference and also the rate of heat transfer is shown in Figure 4.10.
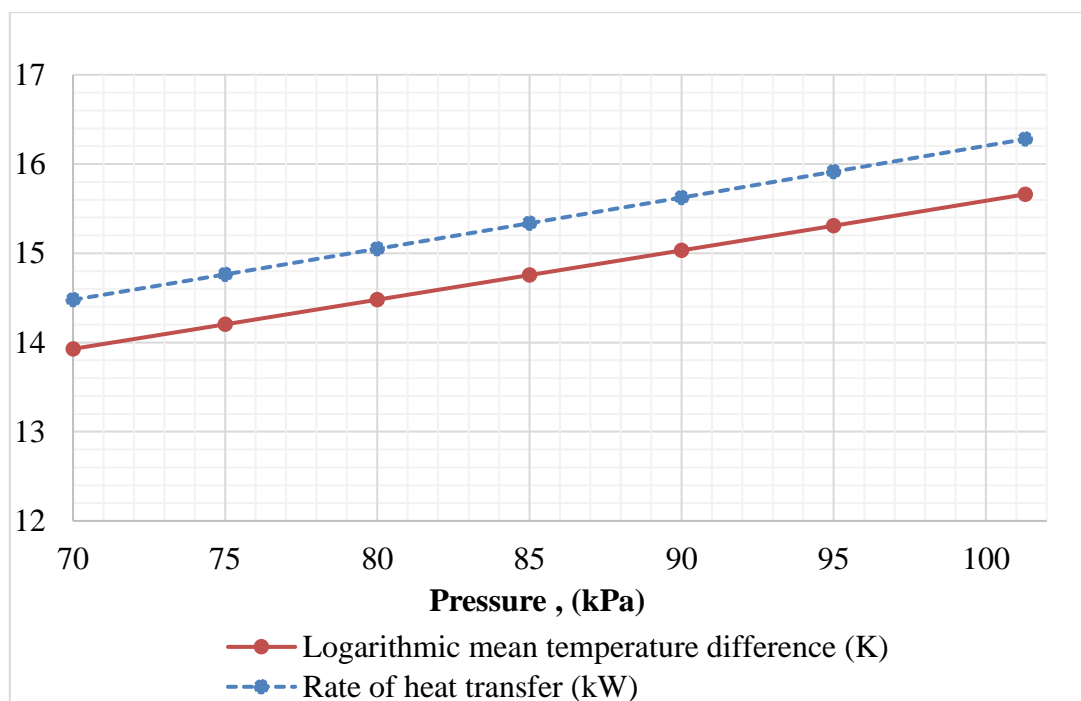
Figure 4.10: Rate of heat transfer and LMTD at different pressure.

From Figure 4.10, both results shows to be linearly dependent. The LMTD and rate of heat transfer will increased linearly with the increased in pressure. This means that at houses that are located at higher altitude, the amount of heat transfer will be much lower compared to those that are near sea level. However, both of the results obtained between the lowest pressure and the highest pressure have slight differences only. Between the lowest and the pressure, the velocity of the outlet air can be determined. The velocity calculated is shown in Figure 4.11.
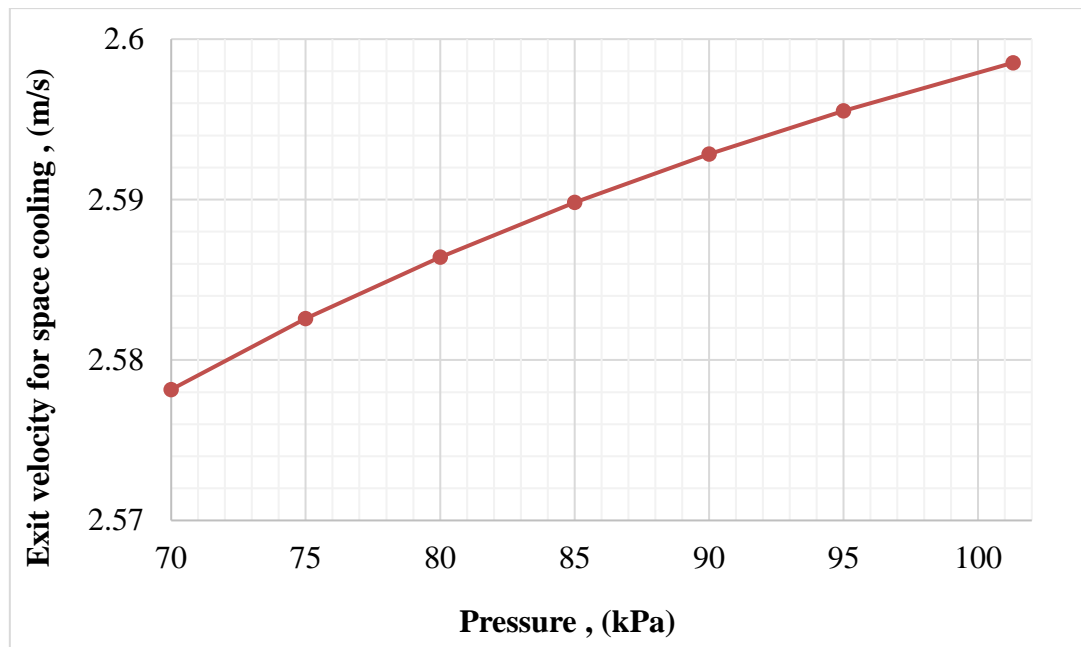
Figure 4.11: Exit velocity for space cooling at different pressure.

The exit velocity for space cooling at each pressure level can be calculated by repeating the previous calculation, that is by multiplying the outlet specific volume with the mass flow rate of dry air. As for the result obtained shown in Figure 4.11, it can be seen that the effect of pressure on the exit velocity is not similar to the relation of LMTD and the rate of heat transfer. With increasing pressure, the exit velocity will increase at a high rate before the increase becoming more gradual. Nontheless, the differences on the exit velocity of air is very minimal, only by 0.02 m/s between a house located at 70 kPa pressure and another house at atmospheric sea level.

There are two important things that need to be taken cautiously. The first is that every calculations done in this section is following the proposed evaporator design. At any point of the day where the inlet dry bulb temperature of air varies with the design, all of the results obtained have to be recalculate. Starting from the changes to enthalpy, specific humidity, specific volume, followed by the water mass balance and finding the energy balance to calculate on the rate of heat transfer, all the way to determine the exit velocity of air for space cooling. Another important thing to consider is that the absorption refrigeration system is not always turned on at any point of the day. Since the solar hot water system is the main priority, the absorption refrigeration system will only be turned on when the hot water in storage tank has met the required temperature.

4.3.2 Coefficient of Performance on the Absorption Refrigeration System

A series of data for the coefficient of performance throughout one day can be obtained by using the temperature of the outlet solar thermal collector and the ambient temperature according to the time of the day. Table 4.1 shows the data obtained.

Table 4.1: The Ambient Temperature and Outlet ST Collector at Each Hour.

Time	Ta, Ambient temperature		Ts, temperature of outlet ST collector	
	°C	K	°C	K
0:00	26	299	26	299
1:00	26	299	26	299
2:00	26	299	26	299
3:00	25	298	25	298
4:00	24	297	24	297
5:00	24	297	24	297
6:00	24	297	31.1	304. 1
7:00	24	297	48.5	321.5
8:00	23	296	59.0	332.0
9:00	25	298	64.6	337.6
10:00	29	302	68.8	341.8
11:00	31	304	71.0	344.0
12:00	33	306	72.1	345.1
13:00	35	308	72.5	345.5
14:00	36	309	71.4	344.4
15:00	36	309	68.8	341.8
16:00	36	309	63.6	336.6
17:00	35	308	51.7	324.7
18:00	30	303	30.9	303.9
19:00	30	303	30	303
20:00	30	303	30	303
21:00	28	301	28	301
22:00	27	300	27	300
23:00	27	300	27	300

With the temperature of both the heat source and the ambient temperature obtained, the coefficient of performance for the absorption refrigeration system can be calculated by using equation (3.23) for each hour. The coefficient of performance is obtained and shown in Figure 4.12.
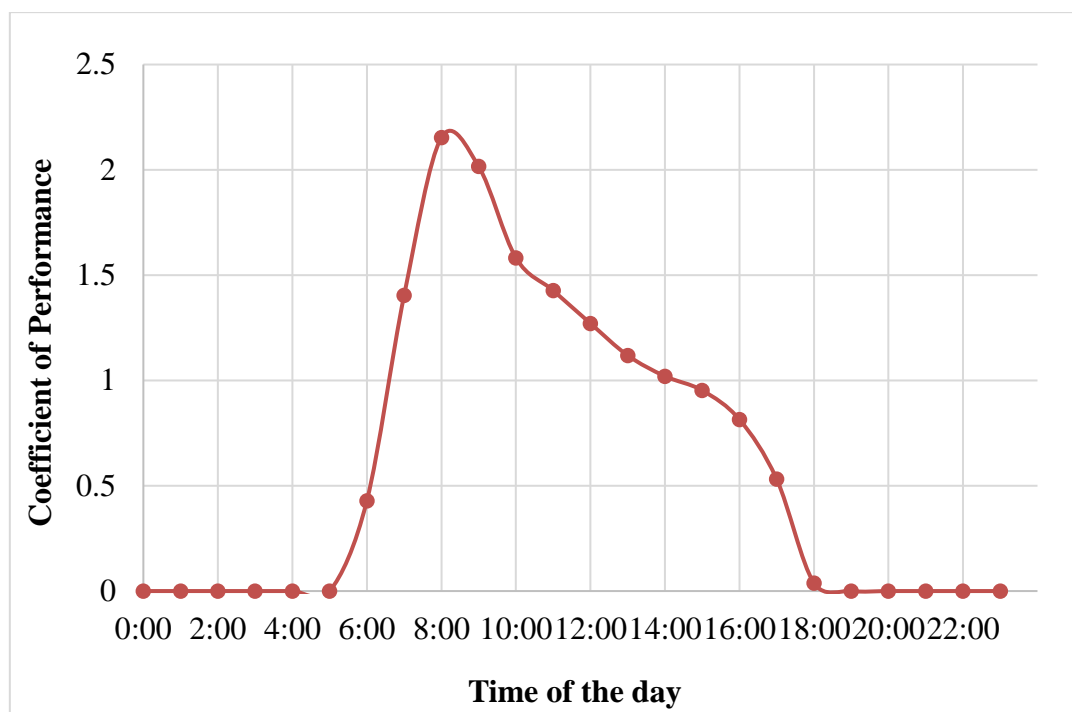
Figure 4.12: COP at different times of the day.

From Figure 4.12, the highest coefficient of performance is having the maximum value at 8:00, which can reach up to 2.2. For a standard absorption refrigeration system, the coefficient of performance is often less than one. This range of coefficient of performance is only obtained from 14:00 to 6:00, which means that this system only requires a very low amount of solar irradiance to achieve the requirements. At higher solar irradiance, which will result in higher temperature of solar thermal collector, the coefficient of performance exceeds the required amount, thus becoming more efficient as compared to other absorption refrigeration system. Based on Figure 4.12, the recommended time for the absorption refrigeration system to operate will be between 7:00 to 15:00. However, the results obtained are based on the assumption that the temperature of the refrigerated space is maintained at -15 °C. Therefore, if the refrigerated space alters, the coefficient of performance have to be recalculate again at each time of the day.

4.4   Return of Investments for Hybrid Photovoltaic Systems

The overall costs of the entire system can be estimated by finding the cost of two separate subsystem available in the market currently. For the solar hot water system, it will cost RM 5250 for the chosen product manufactured by Solar Technology Malaysia, which fits the current design proposed without any further modification on the heat exchanger inside the hot water storage tank. There is no installation cost stated by the manufacturer. Comparing the solar hot water system to instant water heater, a 3.3 kW instant water heater only cost RM 350 with an additional installation fee of RM 50. For a household with eight people, it is assumed that there will be a minimum of six instant water heater installed. Adding the installation fees of all six instant water heater installed, the initial cost for six instant water heater will be RM 3000. Between these two systems, the initial cost of installing instant water heater is cheaper. However, in the long run, the solar water heater system will be much worth since the monthly electricity consumption is lower for solar water heater system.

In order to calculate the variable cost of the instant water heater system, the total time where the heater is turned on has to be determined. The average time spent on one shower is 15 minutes. It is also assumed that a person will have two showers per day. The total time spent on shower would be 240 minutes, which is equivalent to 4 hours per day. By multiplying the power rating of the instant water heater with the total time obtained, the amount of power used that is represented in kilowatts hour can be calculated. There will be a total usage of 13.2 kWh in a day due to instant water heater, which will be around 409.2 kWh in a month.

As for the solar water heater system, provided that the electric booster is only turned on at the maximum solar irradiance hour, the time required to provide additional heating can be used to calculate the total amount of power used in a day. At 13:00, the solar irradiance will be 1030 W/m^2, ambient temperature is 35 °C, collector outlet temperature of 72.5 °C, temperature of hot water produced in storage tank as high as 43.8 °C, and a rate of heat transfer at 8194.1 kJ. The time required at this hour is obtained from Figure 4.6, which is 0.75871 hours. Since the electric booster used has a power rating of 3 kW, the total power used in a day is around 2.28 kWh, and a monthly usage of 70.56 kWh. Since one full tank of water stored is able to deliver hot water shower for the entire day up to eight people, the electric booster is only required to be turned on once per day.

As for the absorption refrigeration system, the fixed initial cost is found to be around RM 5000. There is no variable cost as the space cooling provided is assumed to have operated sufficiently without the needs of turning on the air conditioner at peak solar irradiance hour. However, this fixed cost does not include the cost to install the air ducting. As for the air conditioner, it is assumed that six split unit type air conditioner with 2 hp power rating is operating for 4 hours each day, which will lead to a total usage of 35.79 kWh for each day and a month power usage of 1109.6 kWh.

In order to calculate the electricity cost, the formula is obtained from the stated tariff by Tenaga Nasional Berhad. However, there are different formula for each tariff threshold. The calculations for each variable cost will be shown in Appendix B-4. The variable cost obtained for the electric booster is RM 15.38, instant water heater system is RM 133.35 and RM 515.28 for all six air conditioners used.

With all three variable costs obtained, the brekevenpoint can be found by adding the fixed cost and variable cost for a hybrid photovoltaic system and equal it to the sum of total cost of operating six instant water heater and six air conditioners, which is denoted by system 1 and system 2 respectively. The breakeven point is calculated and shown as follow.

$$Instant\ water\ heating\ system\ =\ RM\ 3000 + (RM\ 133.35\ \times\ t)$$
$$Air\ conditioner\ electricity\ consumption\ =\ (RM\ 515.28\ \times\ t)$$
$$Total\ for\ system\ 1\ =\ RM\ 3000 + (RM\ 133.35\ \times\ t) + (RM\ 515.28\ \times\ t)$$
$$Total\ for\ system\ 1\ =\ RM\ 3000 + (RM\ 648.63\ \times t)$$

$$Solar\ water\ heating\ system\ =\ RM\ 5250 + (RM\ 15.38\ \times\ t)$$
$$Absorption\ refrigeration\ system\ =\ RM\ 5000$$
$$Total\ for\ system\ 2\ =\ RM\ 5250 + (RM\ 15.38 \times t) + RM\ 5000$$
$$Total\ for\ system\ 2\ =\ RM\ 10250 + (RM\ 15.38 \times t)$$

Breakeven point:

$$RM\ 3000 + (RM\ 648.63 \times t) = RM\ 10250 + (RM\ 15.38 \times t)$$

$$633.25 \times t = 7250$$

$$t = \frac{7250}{633.25}$$

$$t = 11.4489\ months$$

From the calculated breakeven point, it takes about 11.4489 months for the proposed hybrid photovoltaic system to overtake the instant water heating system with air conditioners in terms of the cost. Regardless of how efficient the hybrid photovoltaic system can be, the calculation shown is merely an estimate since it is difficult to determine in which hour will the absorption refrigeration system operate at different times of the day. This may cause some variation in the cost of absorption refrigeration system since the usage of air conditioner may be needed. The fixed cost stated previously may also be different from the local price as those are taken from overseas market and converted using the current rate. Also, the electric booster may not be required if the output temperature from solar thermal collector is high enough to increase the temperature of hot water in storage tank above 50 °C. This will ultimately decrease the time required to reach the breakeven point.

CHAPTER 5

CONCLUSIONS AND RECOMMENDATIONS

5.1   Conclusions

For this research project, the heat transfer from each components inside the proposed hybrid photovoltaic systems are analyzed. The photovoltaic thermal collector as well as the solar thermal collector were investigated in order to determine the temperature of the heat carrier through a water channel that will join with either the solar water heating system or the absorption refrigeration system. Since heat generated inside collector will be transferred away, this will lower the collector temperature which will result in achieving a higher efficiency.

The heat exchanger inside the hot water storage tank is designed based on the requirements set, which is to provide a maximum flow rate of 0.125 kg/s and is able to raise the temperature of the water inside the storage tank from 25 °C to 40 °C when the solar thermal collector is supplying hot water at 60 °C for heat exchange. The electric booster which is preinstalled inside the storage tank is able to provide additional heating if required, which will raise the temperature further up to 50 °C. After designing the heat exchanger, a series of data that includes the solar irradiance and ambient temperature for each hour can be used to determine the collector temperature and the temperature of water inside storage tank at each point of the day.

As for the absorption refrigeration system, when water from the outlet of the solar thermal collector enters this system, it is able to cool down any air, thus providing space cooling. Similar to the solar hot water system, the heat exchanger for this system is designed for the evaporator section, which has an intake of air at 37 °C and is able to cool it down to 22 °C. With the heat exchanger designed, it is able to find the coefficient of performance for each hour in order to determine how many hours can the absorption refrigeration system provide space cooling.

In conclusion, both of the applications proposed is able to save the overall costs in the long run if we were to compare these systems with its alternatives such as instant water heaters and air conditioners. Despite the fact that each of these systems proposed will have a high initial fixed cost, the monthly consumptions will be significantly lower. It only takes about 1 year for the proposed systems to breakeven with the alternatives.

5.2 Recommendations for Future Work

It is recommended to have the photovoltaic thermal collector and the solar thermal collector fabricated based on the design proposed in order to obtain the experimental result. This is because there is too many assumptions made previously in the calculations that will not be the case in reality. The temperature of collector obtained practically should be sufficient enough in order to validate the theroretical results. Due to the difficulty in obtaining a real time data for the ambient temperature and solar irradiance, this data can be obtained by setting up the hybrid photovoltaic systems according to the disigns of heat exchanger proposed.

With the real time data obtained, the experimental results on the output temperature of hot water produced in storage tank can be found. It is only then we are able to determine whether the electric booster is required to be turned on or not. The real-time data is crucial in getting an accurate result. This is because the theoretical results obtained previously is assuming that the solar irradiance remains the same for one whole month, which is very unlikely to be true. For the solar hot water system as a whole, the guideline published by Suruhanjaya Tenaga Energy Commision can be studied and implement into the design, such as to include the thermostat temperature which shall not be any lower than 55 °C and not higher than 60 °C. This is to prevent Legionnaire's disease, one of the bacterial infection. It is also stated that isolation barrier have to be installed on the inlet and outlet of the storage tank, which also needed to comply with the requirement provided by MS 1597-2-21:2015.

As for the absorption refrigeration system, it is almost impossible to determine the temperature of the refrigerated space correctly without doing any experiments. This is because the changes in temperature for each components inside the absorption refrigeration system is too complex to be calculated. Therefore, absorption refrigeration system is recommended to be installed before calculating for the coefficient of performance. It is until then, we are able to determine the total number of hours where the absorption refrigeration system is able to provide space cooling for each day. A different absorption refrigeration system can also be further studied in order to compare with the current design. Using chilled water with a fan coil unit instead of air may have a better performance with a downside of harder to maintain. Last but not least, the entire system can try to be installed in other environment, such as condominium to determine a more diverse conclusion on the breakeven point.

REFERENCES

A. L. *et al.,* 2020. 'Theoretical study and indoor experimental validation of performance of the new photovoltaic thermal solar collector (PVT) based water system', *Case Studies in Thermal Engineering*, 18(January), p. 100595. doi: 10.1016/j.csite.2020.100595.

Abdelrazik, A. S. *et al.*, 2019. 'Evaluation of the effects of optical filtration and nanoPCM on the performance of a hybrid photovoltaic-thermal solar collector', *Energy Conversion and Management*, 195(November 2018), pp. 139–156. doi: 10.1016/j.enconman.2019.04.083.

Solar, 2019. *How Do Wind and Humidity Affect Solar Panel Efficiency?* [online] Available at: <https://www.solar.com/learn/how-do-wind-and-humidity-affect-solar-panel-efficiency/> [Accessed April 12, 2021].

United States Environmental Proctection Agency, 2020. *Showerheads*, [online]. Available at: <https://www.epa.gov/watersense/showerheads> [Accessed May 5, 2021].

Summer, *Summer Solar Water Heater Sales & Service Malaysia.*, [online] Available at: <https://www.solartechnologymalaysia.com/solar-water-heater/> [Accessed April 12, 2021].

Buonomano, A., Calise, F. and Palombo, A., 2018. 'Solar heating and cooling systems by absorption and adsorption chillers driven by stationary and concentrating photovoltaic/thermal solar collectors: Modelling and simulation', *Renewable and Sustainable Energy Reviews*, 82(November 2017), pp. 1874–1908. doi: 10.1016/j.rser.2017.10.059.

Çengel Yunus A., Boles, M.A. & Kanoglu, M., 2020. *Thermodynamics: an engineering approach*, Singapore: McGraw-Hill Education.

Chen, Y. *et al.,* 2019. 'Thermo-ecological cost assessment and optimization for a hybrid combined cooling, heating and power system coupled with compound parabolic concentrated-photovoltaic thermal solar collectors', *Energy*, 176, pp. 479–492. doi: 10.1016/j.energy.2019.03.185.

CONCOA, 2012. *Ammonia Properties*, [online] Available at: <https://www.concoa.com/ammonia_properties.html> [Accessed April 12, 2021].

Daghigh, R., Shahidian, R. and Oramipoor, H., 2020. 'A multistate investigation of a solar dryer coupled with photovoltaic thermal collector and evacuated tube collector', *Solar Energy*, 199(February), pp. 694–703. doi: 10.1016/j.solener.2020.02.069.

Dannemand, M. *et al.*, 2020. 'Simulation and optimization of a hybrid unglazed solar photovoltaic-thermal collector and heat pump system with two storage tanks', *Energy Conversion and Management*, 206(January), p. 112429. doi: 10.1016/j.enconman.2019.112429.

Ecavo, 2021. *Solar Energy Disadvantages: The Top Drawbacks of Solar Power*, [online] Available at: <https://ecavo.com/solar-energy-disadvantages/> [Accessed May 5 2021].

Emmi, G. *et al.*, 2020. 'A dynamic analysis of a SAGSHP system coupled to solar thermal collectors and photovoltaic-thermal panels under different climate conditions', *Energy Conversion and Management*, 213(December 2019), p. 112851. doi: 10.1016/j.enconman.2020.112851.

Engineers Edge, L.L.C., 2021. *Overall Heat Transfer Coefficient Table Charts and Equation*, [online] Available at: <https://www.engineersedge.com/thermodynamics/overall_heat_transfer-table.htm> [Accessed April 12, 2021].

Engineers Edge, L.L.C., 2014. Water - Density Viscosity Specific Weight. *Engineers Edge - Engineering, Design and Manufacturing Solutions*, [online] Available at: <https://www.engineersedge.com/physics/water__density_viscosity_specific_weight_13146.htm> [Accessed May 5, 2021].

Engineering ToolBox, 2018. *Ammonia - Density at Varying Temperature and Pressure*, [online] Available at: <https://www.engineeringtoolbox.com/ammonia-density-temperature-pressure-d_2006.html> [Accessed April 12, 2021].

Engineering ToolBox, 2003 *Fluid Heat Transfer Coefficients - Heat Exchanger Surface Combinations*, [online] Available at: https://www.engineeringtoolbox.com/overall-heat-transfer-coefficients-d_284.html [Accessed April 12, 2021].

EnggCyclopedia, 2020. *Shell & tube heat exchanger equations and calculations*, [online] Available at: <https://www.enggcyclopedia.com/2019/05/shell-tube-heat-exchanger-equations/> [Accessed April 12, 2021].

Klevinskis, A. and Bučinskas, V., 2011. 'Analysis of a Flat-Plate Solar Collector', *Mokslas - Lietuvos ateitis*, 3, pp. 39–43.

Li, M. *et al.*, 2020. 'Photovoltaic thermal module and solar thermal collector connected in series: Energy and exergy analysis', *Energy Conversion and Management*, 206(January), p. 112479. doi: 10.1016/j.enconman.2020.112479.

Li, Z. *et al.*, 2020. 'Comprehensive evaluation of low-grade solar trigeneration system by photovoltaic-thermal collectors', *Energy Conversion and Management*, 215(January), p. 112895. doi: 10.1016/j.enconman.2020.112895.

Liu, L. *et al.*, 2017. 'Performance evaluation of a novel solar photovoltaic–thermal collector with dual channel using microencapsulated phase change slurry as cooling fluid', *Energy Conversion and Management*, 145, pp. 30–40. doi: 10.1016/j.enconman.2017.04.089.

Ma, T., Li, M. and Kazemian, A., 2020. 'Photovoltaic thermal module and solar thermal collector connected in series to produce electricity and high-grade heat simultaneously', *Applied Energy*, 261(June 2019), p. 114380. doi: 10.1016/j.apenergy.2019.114380.

Mellor, A. *et al.*, 2018. 'Roadmap for the next-generation of hybrid photovoltaic-thermal solar energy collectors', *Solar Energy*, 174(February), pp. 386–398. doi: 10.1016/j.solener.2018.09.004.

Pang, W. *et al.*, 2020. 'Enhanced electrical performance for heterojunction with intrinsic thin-layer solar cells based photovoltaic thermal system with aluminum collector', *International Communications in Heat and Mass Transfer*, 116(June), p. 104705. doi: 10.1016/j.icheatmasstransfer.2020.104705.Abdullah.

Primo, J., 2012. *'PDHonline Course M371 (2 PDH) Shell and Tube Heat Exchangers Basic Calculations'*, 371, pp. 3–4.

PVEducation, 2021. *Calculation of Solar Insolation.* Available at: <https://www.pveducation.org/pvcdrom/properties-of-sunlight/calculation-of-solar-insolation> [Accessed April 12, 2021].

Raja, A. A. and Huang, Y., 2020. 'Novel parabolic trough solar collector and solar photovoltaic/thermal hybrid system for multi-generational systems', *Energy Conversion and Management*, 211(December 2019), p. 112750. doi: 10.1016/j.enconman.2020.112750.

Ramdani, H. and Ould-Lahoucine, C., 2020. 'Study on the overall energy and exergy performances of a novel water-based hybrid photovoltaic-thermal solar collector', *Energy Conversion and Management*, 222(May), p. 113238. doi: 10.1016/j.enconman.2020.113238.

Agbo, S.N. and Okoroigwe, E.C., 2007. *Analysis of Thermal Losses in the Flat-Plate Collector of a Thermosyphon Solar Water Heater*, [online] Available at: <https://scialert.net/fulltext/?doi=rjp.2007.35.41> [Accessed April 12, 2021].

Su, D. *et al.*, 2017. 'Comparative analyses on dynamic performances of photovoltaic–thermal solar collectors integrated with phase change materials', *Energy Conversion and Management*, 131, pp. 79–89. doi: 10.1016/j.enconman.2016.11.002.

Timeanddate, 2021. *Hour-by-Hour Forecast for Kuala Lumpur, Malaysia*, [online] Available at: <https://www.timeanddate.com/weather/malaysia/kuala-lumpur/hourly> [Accessed May 5, 2021].

The ASEAN Post, 2019. *Malaysia's solar sector on the rise*, [online] Available at: <https://theaseanpost.com/article/malaysias-solar-sector-rise> [Accessed April 12, 2021].

Thinsurat, K. *et al.*, 2019. 'Performance study of solar photovoltaic-thermal collector for domestic hot water use and thermochemical sorption seasonal storage', *Energy Conversion and Management*, 180(November 2018), pp. 1068–1084. doi: 10.1016/j.enconman.2018.11.049.

Zaite, A. *et al.*, 2020. 'Photovoltaic–thermal collectors for night radiative cooling and solar heating: Numerical study', *Materials Today: Proceedings*, (xxxx). doi: 10.1016/j.matpr.2020.04.352.

Zarei, A. *et al.*, 2020. 'A Novel, eco-friendly combined solar cooling and heating system, powered by hybrid Photovoltaic thermal (PVT) collector for domestic application', *Energy Conversion and Management*, 222(July), p. 113198. doi: 10.1016/j.enconman.2020.113198.

APPENDICES

APPENDIX A: Figures
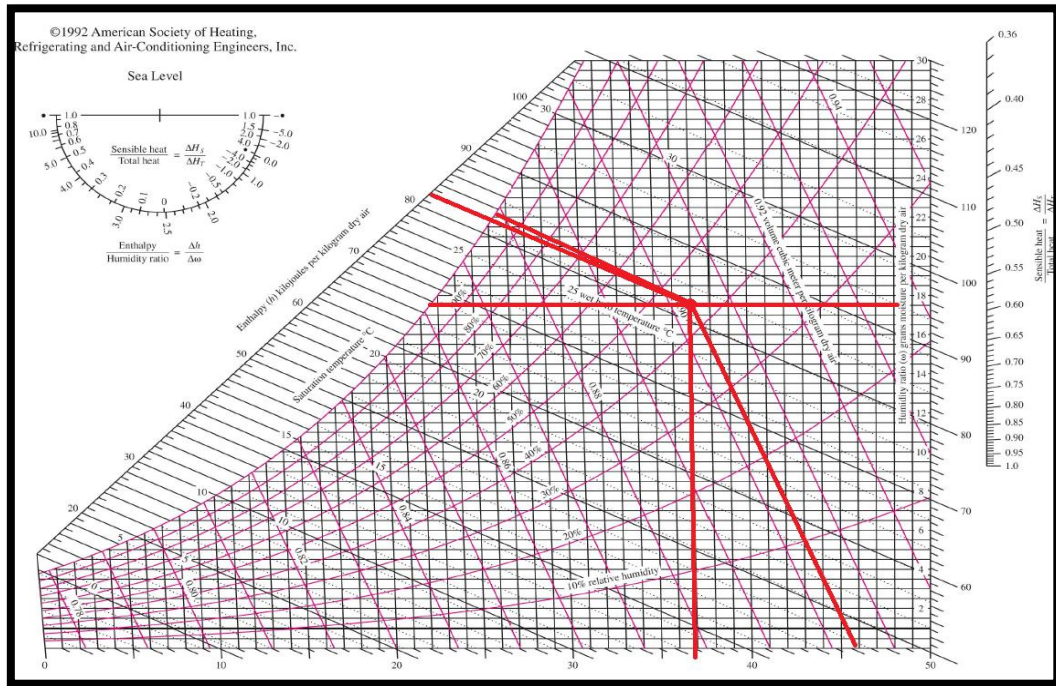
Figure A-1: The results obtained for the inlet air.
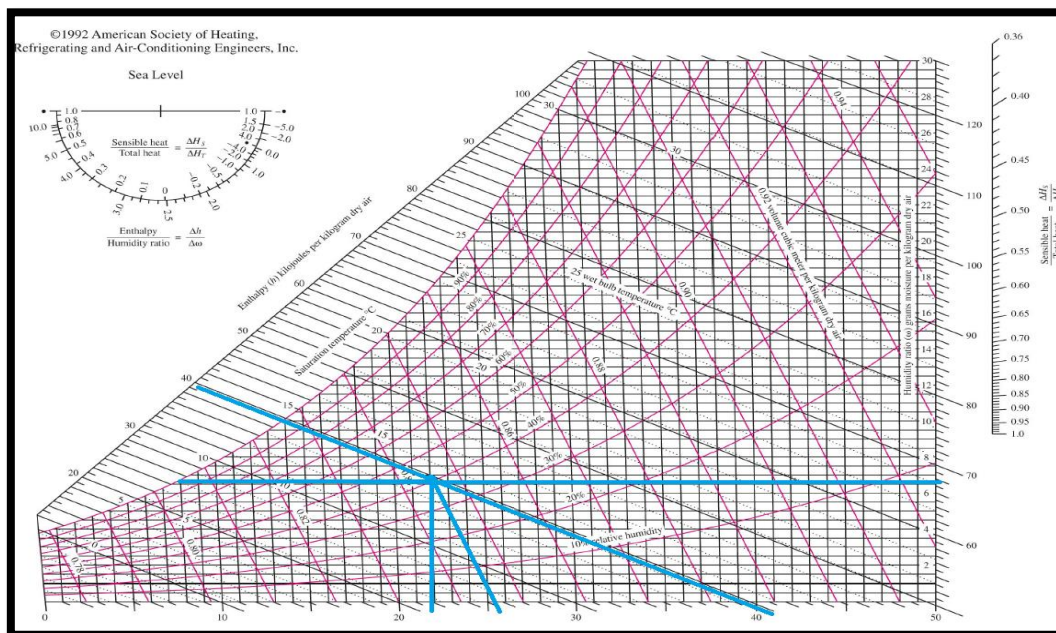
Figure A-2: The results obtained for the outlet air.

APPENDIX B: Calculations

Appendix B-1: The theoretical calculations at 1 atmospheric pressure.

$$P_{v1} = \varphi_1 \, P_{g1} = \varphi_1 \, P_{sat@37\,°C}$$
$$P_{v1} = 0.44 \times 6.3315 \, kPa$$
$$P_{v1} = 2.78586 \, kPa$$

$$T_{dp1} = T_{sat@2.78586\,kPa}$$
$$T_{dp1} = 22.6888 \,°C$$

$$P_{a1} = P_1 - P_{v1}$$
$$P_{a1} = 101.3 \, kPa - 2.78586 \, kPa$$
$$P_{a1} = 98.5141 \, kPa$$

$$P_{a1}v_1 = RT$$
$$v_1 = \frac{RT}{P_{a1}}$$
$$v_1 = \frac{(0.287 \, kPa.\,m^3/kgK)(310 \, K)}{(98.5141 \, kPa)}$$
$$v_1 = 0.90312 \, m^3/kg \, dry \, air$$

$$\omega_1 = \frac{0.622 \times P_{v1}}{P_1 - P_{v1}}$$
$$\omega_1 = \frac{0.622 \times 2.78586 \, kPa}{101.3 \, kPa - 2.78586 \, kPa}$$
$$\omega_1 = 0.01759 \, kg \, water/kg \, dry \, air$$

$$h_{g1} = h_{g@37\,°C} = 2541.04 \, kJ/kg \, dry \, air$$
$$h_1 = CpT_1 + \omega_1 h_{g1}$$
$$h_1 = \left(1.005 \frac{kJ}{kg}.K\right)(310 \, K) + \left(0.01759 \frac{kg \, water}{kg \, dry \, air}\right)\left(2541.04 \frac{kJ}{kg \, dry \, air}\right)$$
$$h_1 = 82.3574 \, kJ/kg \, dry \, air$$

$$P_{v2} = P_{sat@8\,°C} = 1.08586\ kPa$$

$$P_{a2} = P_1 - P_{v2}$$

$$P_{a2} = 101.3\ kPa - 1.08586\ kPa$$

$$P_{a2} = 100.214\ kPa$$

$$P_{a2}v_2 = RT$$

$$v_2 = \frac{RT}{P_{a2}}$$

$$v_2 = \frac{(0.287\ kPa.m^3/kgK)(295\ K)}{(100.214\ kPa)}$$

$$v_2 = 0.84484\ m^3/kg\ dry\ air$$

$$\omega_2 = \frac{0.622 \times P_{v2}}{P_1 - P_{v2}}$$

$$\omega_2 = \frac{0.622 \times 1.08586\ kPa}{101.3\ kPa - 1.08586\ kPa}$$

$$\omega_2 = 0.00674\ kg\ water/kg\ dry\ air$$

$$h_{g2} = h_{g@22\,°C} = 2541.04\ kJ/kg\ dry\ air$$

$$h_2 = CpT_2 + \omega_2 h_{g2}$$

$$h_2 = \left(1.005\ \tfrac{kJ}{kg}.K\right)(295\ K) + \left(0.00674\ \tfrac{kg\ water}{kg\ dry\ air}\right)\left(2541.04\ \tfrac{kJ}{kg\ dry\ air}\right)$$

$$h_2 = 39.2356\ kJ/kg\ dry\ air$$

Volumetric flow rate of inlet ducting:

$$A = \pi r^2$$

$$A = \pi \times (0.2\ m)^2$$

$$A = 0.12566\ m^2$$

$$V = 10\ km/h = 2.7778\ m/s$$

$$\dot{v} = AV$$

$$\dot{v} = 0.12566\ m^2 \times 2.7778\ m/s$$

$$\dot{v} = 0.34906\ m^3/s$$

Mass flow rate of dry air inside ducting:

$$\dot{m}_a = \frac{\dot{v}}{v_2}$$

$$\dot{m}_a = \frac{0.34906 \; m^3/s}{0.84484 \; m^3/kg \; dry \; air}$$

$$\dot{m}_a = 0.3865 \; kg/s$$

Water mass balance:

$$\sum \dot{m}_{w,i} = \sum \dot{m}_{w,e}$$

$$\dot{m}_w = \dot{m}_a(\omega_1 - \omega_2)$$

$$\dot{m}_w = 0.3865 \; \frac{kg}{s} \times \left(0.01759 \; \frac{kg \; water}{kg \; dry \; air} - 0.00674 \; \frac{kg \; water}{kg \; dry \; air} \right)$$

$$\dot{m}_w = 0.00419 \; kg/s$$

Energy balance on control volume:

$$h_{w2} = h_{f@22 \, °C} = 92.281 \; kJ/kg$$

$$\sum \dot{m}_i h_i = \sum \dot{m}_e h_e + \dot{Q}_{out}$$

$$\dot{Q}_{out} = \dot{m}_a(h_1 - h_2) - \dot{m}_w h_{w2}$$

$$\dot{Q}_{out} = \left(0.3865 \; \frac{kg}{s} \right) (82.3574 - 39.2356) \frac{kJ}{kg \; dry \; air} - \left(0.00419 \frac{kg}{s} \right) \left(92.281 \frac{kJ}{kg} \right)$$

$$\dot{Q}_{out} = 16.2796 \; kW$$

Exit velocity of air inside ducting:

$$\dot{v} = \dot{m} v_2 = (0.3865 \; kg/s)(0.84484 \; m^3/kg \; dry \; air)$$

$$\dot{v} = 0.32653 \; m^3/s$$

$$V = \frac{\dot{v}}{A} = \frac{0.32653 \; m^3/s}{0.12566 \; m^2}$$

$$V = 2.59853 \; m/s$$

Mass flow rate of refrigerant:

$$\dot{m}_{ref} = \frac{\dot{Q}_{out}}{Cp \Delta T}$$

$$\dot{m}_{ref} = \frac{16.2796 \; kW}{(2.2 \; kJ/kg.K)(17 \, °C - 10 \, °C)} = 1.05712 \; kg/s$$

Appendix B-2: Temperature of water inside storage tank.

The area of heat transfer remains constant,

$A = 1.9481 \, m^2$

Number of tubes inside heat exchanger: 2 tubes with 10 tube passes.

$$\dot{m}C_p\Delta T = U \times A \times LMTD$$

$$\dot{m}C_p(t_2 - t_1) = U \times A \times \left[\frac{(T_1 - t_2) - (T_2 - t_1)}{\ln\left[\frac{(T_1 - t_2)}{(T_2 - t_1)}\right]}\right]$$

$$\left(0.125\frac{kg}{s}\right)\left(4.2\frac{kJ}{kg}.K\right)(t_2 - 25\,°C) = 397.5\frac{W}{m^2K} \times 1.9481\,m^2 \times \left[\frac{(48.49946\,°C - t_2) - (30\,°C - 25\,°C)}{\ln\left[\frac{(48.49946\,°C - t_2)}{(30\,°C - 12\,°C)}\right]}\right]$$

By using trial and error,

$t_2 = 36.2276\,°C$

Appendix B-3: Temperature of water inside storage tank with lower mass flow rate.

The area of heat transfer remains constant,

$A = 1.9481 \, m^2$

Number of tubes inside heat exchanger: 2 tubes with 10 tube passes.

$\dot{m}C_p\Delta T = U \times A \times LMTD$

$$\dot{m}C_p(t_2 - t_1) = U \times A \times \left[\frac{(T_1 - t_2) - (T_2 - t_1)}{\ln\left[\frac{(T_1 - t_2)}{(T_2 - t_1)}\right]}\right]$$

$$\left(0.05\,\frac{kg}{s}\right)\left(4.2\,\frac{kJ}{kg}.K\right)(t_2 - 25\,°C) = 397.5\,\frac{W}{m^2K} \times 1.9481\,m^2 \times \left[\frac{(48.49946\,°C - t_2) - (30\,°C - 25\,°C)}{\ln\left[\frac{(48.49946\,°C - t_2)}{(30\,°C - 12\,°C)}\right]}\right]$$

By using trial and error,

$t_2 = 43.0673\,°C$

Appendix B-4: The electricirt tariff provided by Tenaga Nasional Berhad.

For instant water heater system,

$Monthly\ electricity\ consumption:$

$For\ first\ 200\ kWh,$

$$Consumption = \frac{200\ kWh\ \times 21.80}{100}$$

$Consumption = RM\ 43.60$

$For\ the\ next\ 100\ kWh,$

$$Consumption = \frac{100\ kWh\ \times 33.40}{100}$$

$Consumption = RM\ 33.40$

$For\ the\ next\ 300\ kWh,$

$$Consumption = \frac{(409.2\ kWh\ -\ 300\ kWh)\ \times 51.60}{100}$$

$Consumption = RM\ 56.35$

$Total\ consumption = RM\ 43.60 + RM\ 33.40 + RM\ 56.35$

$Total\ consumption = RM\ 133.35$

For solar hot water system,

$Monthly\ electricity\ consumption:$

$For\ P_{mothly} < 200\ kWh,$

$$Consumption = \frac{P_{mothly}\ \times 21.80}{100}$$

$$Consumption = \frac{70.56\ kWh\ \times 21.80}{100}$$

$Consumption = RM\ 15.38$

For air conditioners,

Monthly electricity consumption:

For first $200\ kWh$,

$$Consumption = \frac{200\ kWh\ \times 21.80}{100}$$

$Consumption =\ RM\ 43.60$

For the next $100\ kWh$,

$$Consumption = \frac{100\ kWh\ \times 33.40}{100}$$

$Consumption =\ RM\ 33.40$

For the next $300\ kWh$,

$$Consumption = \frac{300\ kWh\ \times 51.60}{100}$$

$Consumption =\ RM\ 154.80$

For the next $300\ kWh$,

$$Consumption = \frac{300\ kWh\ \times 54.60}{100}$$

$Consumption =\ RM\ 163.80$

Next $901\ kWh\ onwards$,

$$Consumption = \frac{(1109.6 - 900\ kWh)\ \times 57.10}{100}$$

$Consumption =\ RM\ 119.68$

$Total\ consumption =\ RM\ 43.60 + RM\ 33.40 + RM\ 56.35 + RM\ 154.80 +$

$RM\ 163.80 + RM\ 119.68$

$Total\ consumption =\ RM\ 515.28$

APPENDIX C: Table

Table C-1: The Energy Required to Heat a Full Tank of Water to 50 °C.

Time of the day	Temperature of water tank before heating with electric booster (°C)	Energy required to heat a full tank to 50 °C (kJ)
0:00	26	31651.2
1:00	26	31651.2
2:00	26	31651.2
3:00	25	32970
4:00	24	34288.8
5:00	24	34288.8
6:00	29.3	27286.2
7:00	36.2	18163
8:00	39.7	13594.5
9:00	41.4	11317.8
10:00	42.7	9613.59
11:00	43.3	8777.93
12:00	43.7	8330.73
13:00	43.8	8194.1
14:00	43.5	8601.74
15:00	42.7	9618.93
16:00	41.1	11696.2
17:00	37.3	16726.9
18:00	29.2	27401.5
19:00	30	26376
20:00	30	26376
21:00	28	29013.6
22:00	27	30332.4
23:00	27	30332.4